INTERNATIONAL JOURNAL FOR NUMERICAL METHODS IN FLUIDS, VOL. 25, 1315–1344 (1997)

UNSTEADY INCOMPRESSIBLE FLOWS PAST TWO CYLINDERS IN TANDEM AND STAGGERED ARRANGEMENTS

S. MITTAL,[1]* V. KUMAR[1] AND A. RAGHUVANSHI[2]

[1] *Department of Aerospace Engineering, Indian Institute of Technology, Kanpur, UP 208 016, India.*
[2] *Tata Consultancy Services, India*

SUMMARY

A stabilized finite element formulation is employed to study incompressible flows past a pair of cylinders at Reynolds numbers 100 and 1000 in tandem and staggered arrangements. Computations are carried out for three sets of cylinder arrangements. In the first two cases the cylinders are arranged in tandem and the distance between their centres is 2·5 and 5·5 diameters. The third case involves the two cylinders in staggered arrangement. The distance between their centres along the flow direction is 5·5 diameters, while it is 0·7 diameter in the transverse direction. The results are compared with flows past a single cylinder at corresponding Reynolds numbers and with experimental observations by other researchers. It is observed that the qualitative nature of the flow depends strongly on the arrangement of cylinders and the Reynolds number. In all cases, when the flow becomes unsteady, the downstream cylinder, which lies in the wake of the upstream one, experiences very large unsteady forces that may lead to wake-induced flutter. The Strouhal number, based on the dominant frequency in the time history of the lift coefficient, for both cylinders attains the same value. In some cases, even though the near wake of the two cylinders shows temporal periodicity, the far wake does not. © 1997 John Wiley & Sons, Ltd.

Int. J. Numer. Meth. Fluids, **25**: 1315–1344 (1997)

No. of Figures: 23. No. of Tables: 1. No. of References: 21.

KEY WORDS: finite element; two cylinders; unsteady flows; vortex shedding

1. INTRODUCTION

Fluid dynamic interaction between two cylinders is an important phenomenon in engineering flows; for example, it occurs in flows that involve offshore structures, transmission cables with twin conductors, twin chimney stacks and heat exchanger tubes. The arrangement of the cylinders with respect to the freestream flow direction can be broadly classified as tandem (or in-line), transverse (or side-by-side) or staggered. Significant research has gone into the understanding of flows past cylinders in transverse arrangement.[1,2] Kim and Durbin[3] investigated experimentally the flow past a pair of cylinders in transverse arrangement when the flow is in the flopping regime. They also studied the effect of a splitter plate along the centreline of the cylinders as a flow control mechanism. Tokunaga *et al.*[4] computed flows past two cylinders in transverse arrangement and compared their

* Correspondence to: S. Mittal, Department of Aerospace Engineering, Indian Institute of Technology, Kanpur, UP 208 016, India.

Contract grant sponsor: Department of Science and Techanology, India; Contract grant number: DST-AE-95279

CCC 0271–2091/97/111315–30 $17.50

Received 26 August 1996
Revised 22 January 1997

results with flow visualization results of Williamson.[5] A detailed numerical investigation, along similar lines, of the flow past a pair of flat plates normal to the flow was carried out by Behr *et al.*[6] Experimental results for flows past two cylinders in-line and staggered arrangements have been reported by Zdravkovich,[1] Chen[2] and Kiya *et al.*[7,8] Kiya *et al.*[7] carried out a systematic study to investigate the flow interference between two cylinders in various arrangements with distances between their centres less than 5 cylinder diameters. Based on their experimental findings, they reported that for the in-line arrangement, if the spacing between the two cylinders is less than a certain critical value, no distinct vortex shedding is observed downstream of the first cylinder. However, a vortex sheet is formed downstream of the second cylinder. This critical distance was found to be approximately 3 cylinder diameters. They were also able to draw a contour map of the variation in the Strouhal number with respect to the arrangement of the two cylinders. In another piece of work, Kiya *et al.*[8] carried out experiments on the flow past two cylinders in tandem with the distance between their centres as 3·47 diameters. They observed two distinct flow patterns which switch randomly in time. The average time interval for the two patterns is strongly dependent on the turbulent intensity. Interestingly, the distance between the two cylinders is quite close to the critical spacing that they reported in an earlier paper.[8] Numerical simulation of flows past periodic arrays of staggered cylinders was reported by Johnson *et al.*[9] They computed uniperiodic flows with each cell of periodicity consisting of either two or 10 cylinders. Biperiodic flows were computed with two cylinders in each cell of periodicity. They established that the steady state flows (computed by dropping the time-derivative terms from the governing equations) result in a significantly different solution compared with the time-averaged temporally periodic unsteady solutions. It should be pointed out that most of the experimental research reported in the literature has been conducted at Reynolds numbers exceeding 10^4, while the numerical results have been reported for flows at Reynolds number 100. Despite the Reynolds numbers for the computations being significantly lower than those encountered in practical situations, they are of immense help in understanding the underlying physical phenomena.

In this paper we report our computational results for flows past two cylinders in staggered and in-line arrangements at Reynolds numbers 100 and 1000. The first case involves the two cylinders in tandem with a distance of 2·5 diameters between their centres. At *Re* 100 our computations lead to a steady solution, while an unsteady solution is realized at *Re* 1000. In the second set of computations the distance between the centre of the cylinders is increased to 5·5 diameters. As suggested by the experimental observations discussed above, it is expected that the flows for these two cylinder arrangements will be qualitatively different with respect to the vortex shedding. To study the fluid dynamic interference effect of the two cylinders, the solutions are also compared with flows past a single cylinder at the respective Reynolds numbers. The flow past a circular cylinder at *Re* 100 has become a standard benchmark problem and various researchers in the past have reported computed results which are in good agreement with experimental observations.[10–13] In this paper the flow past a single cylinder at *Re* 1000 is computed and compared with experimental observations and results from other computations. The last set of computations is carried out for flows that involve two cylinders in staggered arrangement. The cylinders are arranged such that the in-line distance between their centres remains the same as in the previous case (5·5 diameters), while the transverse distance is set to 0·7 diameter.

The outline of the rest of the paper is as follows. We begin by reviewing the governing equations for incompressible fluid flow in Section 2. The SUPG (streamline upwind/Petrov–Galerkin) and PSPG (pressure-stabilizing/Petrov–Galerkin) stabilization technique[10,14,15] is employed to stabilize our computations against spurious numerical oscillations and to enable us to use equal-order-interpolation velocity–pressure elements. Section 3 describes the finite element formulation incorporating these stabilizing terms. In Section 4 we present our computational results for flows

involving a single cylinder and a pair of cylinders in tandem and staggered arrangements. In Section 5 we summarize the results and make some concluding remarks.

2. GOVERNING EQUATIONS

Let $\Omega \subset \mathbb{R}^{n_{sd}}$ and $(0, T)$ be the spatial and temporal domains respectively, where n_{sd} is the number of space dimensions, and let Γ denote the boundary of Ω. The spatial and temporal co-ordinates are denoted by $\mathbf{x}$ and t respectively. The Navier–Stokes equations governing incompressible fluid flow are

$$\rho\left(\frac{\partial \mathbf{u}}{\partial t}\right) + \mathbf{u} \cdot \nabla \mathbf{u} - \mathbf{f}) - \nabla \cdot \boldsymbol{\sigma} = 0 \quad \text{on } \Omega \text{ for } (0, T), \tag{1}$$

$$\nabla \cdot \mathbf{u} = 0 \quad \text{on } \Omega \text{ for } (0, T). \tag{2}$$

Here ρ, $\mathbf{u}$, $\mathbf{f}$ and $\boldsymbol{\sigma}$ are the density, velocity, body force and stress tensor respectively. The stress tensor is written as the sum of its isotropic and deviatoric parts:

$$\boldsymbol{\sigma} = -p\mathbf{I} + \mathbf{T}, \qquad \mathbf{T} = 2\mu\boldsymbol{\varepsilon}(\mathbf{u}), \qquad \boldsymbol{\varepsilon}(\mathbf{u}) = \frac{1}{2}[(\nabla \mathbf{u}) + (\nabla \mathbf{u})^{\mathrm{T}}], \tag{3}$$

where p and μ are the pressure and viscosity respectively. Both Dirichlet and Neumann-type boundary conditions are accounted for, represented as

$$\mathbf{u} = \mathbf{g} \quad \text{on } \Gamma_g, \qquad \mathbf{n} \cdot \boldsymbol{\sigma} = \mathbf{h} \quad \text{on } \Gamma_h, \tag{4}$$

where Γ_g and Γ_h are complementary subsets of the boundary Γ. The initial condition on the velocity is specified on Ω:

$$\mathbf{u}(\mathbf{x}, 0) = \mathbf{u}_0 \quad \text{on } \Omega, \tag{5}$$

where $\mathbf{u}_0$ is divergence-free.

3. FINITE ELEMENT FORMULATION

Consider a finite element discretization of Ω into subdomains Ω^e, $e = 1, 2, \ldots, n_{el}$, where n_{el} is the number of elements. Based on this discretization, for velocity and pressure we define the finite element trial function spaces $\mathscr{S}^h_{\mathbf{u}}$ and $\mathscr{S}^h_p$ and weighting function spaces $\mathscr{V}^h_{\mathbf{u}}$ and $\mathscr{V}^h_p$. These function spaces are selected, by taking the Dirichlet boundary conditions into account, as subsets of $[\mathbf{H}^{1h}(\Omega)]^{n_{sd}}$ and $\mathbf{H}^{1h}(\Omega)$, where $\mathbf{H}^{1h}(\Omega)$ is the finite-dimensional function space over Ω. The stabilized finite element formulation of (1) and (2) is written as follows: find $\mathbf{u}^h \in \mathscr{S}^h_{\mathbf{u}}$ and $p^h \in \mathscr{S}^h_p$ such that $\forall^h_{\mathbf{w}} \in \mathscr{V}^h_{\mathbf{u}}$, $q^h \in \mathscr{V}^h_p$

$$\begin{aligned}\int_\Omega \mathbf{w}^h \cdot \rho\left(\frac{\partial \mathbf{u}^h}{\partial t} + \mathbf{u}^h \cdot \nabla \mathbf{u}^h - \mathbf{f}\right) \mathrm{d}\Omega + \int_\Omega \boldsymbol{\varepsilon}(\mathbf{w}^h) : \boldsymbol{\sigma}(p^h, \mathbf{u}^h)\, \mathrm{d}\Omega + \int_\Omega q^h \nabla \cdot \mathbf{u}^h\, \mathrm{d}\Omega \\ + \sum_{e=1}^{n_{el}} \int_{\Omega^e} \frac{1}{\rho}(\tau_{SUPG}\rho \mathbf{u}^h \cdot \nabla \mathbf{w}^h + \tau_{PSPG} \nabla q^h) \\ \times \left[\rho\left(\frac{\partial \mathbf{u}^h}{\partial t} + \mathbf{u}^h \cdot \nabla \mathbf{u}^h - \mathbf{f}\right) - \nabla \cdot \boldsymbol{\sigma}(p^h, \mathbf{u}^h)\right] \mathrm{d}\Omega^e \\ + \sum_{e=1}^{n_{el}} \int_{\Omega^e} \delta \nabla \cdot \mathbf{w}^h \rho \nabla \cdot \mathbf{u}^h\, \mathrm{d}\Omega^e = \int_{\Gamma_h} \mathbf{w}^h \cdot \mathbf{h}^h\, \mathrm{d}\Gamma.\end{aligned} \tag{6}$$

Remarks

1. In the variational formulation given by (6), the first three terms and the right-hand side constitute the Galerkin formulation of the problem.
2. The first series of element-level integrals comprises the SUPG and PSPG stabilization terms added to the variational formulations.[10,11] In the current formulation, τ_{PSPG} is the same as τ_{SUPG} and is given as

$$\tau = \left[\left(\frac{2\|\mathbf{u}^h\|}{h} \right)^2 + \left(\frac{4\nu}{h^2} \right)^2 \right]^{-1/2}. \tag{7}$$

3. The second series of element-level integrals is added to the formulation for numerical stability at high Reynolds numbers. This is a least squares term based on the continuity equation. The coefficient δ is defined as

$$\delta = \frac{h}{2}\|\mathbf{u}^h\| z, \tag{8}$$

where

$$z = \begin{cases} Re_u/3, & Re_u \leqslant 3, \\ 1, & Re_u > 3, \end{cases} \tag{9}$$

and Re_u is the cell Reynolds number.
4. Both stabilization terms are weighted residuals and therefore maintain the consistency of the formulation.

4. NUMERICAL SIMULATIONS

All the computations reported in this paper are carried out on the Digital workstations at IIT Kanpur. Equal-in-order bilinear basis functions for velocity and pressure are used and 2×2 Gaussian quadrature is employed for numerical integration. The non-linear equation systems resulting from the finite element discretization of the flow equations are solved using the generalized minimal residual (GMRES) technique[16] in conjunction with diagonal preconditioners. The two equal-sized cylinders reside in a rectangular computational domain whose upstream boundary is located at 5 cylinder diameters from the centre of the first cylinder. The downstream boundary is located at 16 cylinder diameters from the centre of the second cylinder. The upper and lower boundaries are placed at 8 diameters from the centre of the first cylinder. The no-slip condition is specified for the velocity on the cylinder wall and freestream values are assigned for the velocity at the upstream boundary. At the downstream boundary we specify a Neumann-type boundary condition for the velocity that corresponds to zero viscous stress vector. On the upper and lower boundaries the component of velocity normal to and the component of stress vector along these boundaries is prescribed zero value. The Reynolds number is based on the diameter of the cylinders, the freestream velocity and the viscosity of the fluid. Computations are carried out for various relative locations of the two cylinders. The non-dimensional distance between the centres of the two cylinders is denoted by P/D in the flow direction and by T/D in the cross-flow direction as shown in Figure 1. In the rest of the paper we will refer to the upstream cylinder as cylinder 1 and to the downstream one as cylinder 2.

Computations are carried out for three sets of cylinder arrangements and two values of Reynolds number. The Reynolds numbers considered are 100 and 1000. In two of the three cases the two cylinders are arranged in tandem with $T/D = 0$ and $P/D = 2{\cdot}5$ and $5{\cdot}5$, while the third case is that of

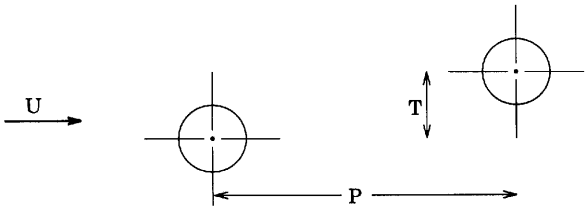

Figure 1. Description of relative location of two cylinders

staggered arrangement of the two cylinders with $T/D = 0{\cdot}7$ and $P/D = 5{\cdot}5$. The results are also compared with flows past a single cylinder at the respective Reynolds numbers. In all cases, first the steady state solution is computed for the flow past a cylinder at $Re = 100$. This solution is then perturbed by applying, on the upstream cylinder, a belt-type boundary condition that consists of a set of counter-clockwise and clockwise rotations. Computations are carried out till a periodic solution develops. The unsteady solution at *Re* 100 is used as an initial condition for computing the flow at *Re* 1000. The finite element mesh consists of approximately 8000 elements. A view of the mesh for the case of staggered arrangement of the two cylinders is shown in Figure 2.

4.1. Re 1000 flow past a single cylinder

To understand the effect of placing a second cylinder in the flow field, it is essential to first study the flow past a single cylinder. The flow past a circular cylinder at *Re* 100 has become a standard benchmark problem and various researchers in the past have reported computed results which are in good agreement with experimental observations.[10–13] Here we report the flow past a single cylinder at *Re* 1000. The finite element mesh consists of 6181 nodes and 6000 quadrilateral elements. Figures 3 and 4 show the vorticity streamfunction and pressure fields during one cycle of the lift coefficient. We observe that, compared with the flow at *Re* 100,[10,11] the vortices are stronger and the lateral spacing between them in the wake is significantly smaller. Additionally, secondary vortices are generated in the *Re* 1000 case as a result of the interaction between primary vortices and the cylinder wall; they are absent in the case of *Re* 100 flow. Figure 5 shows the time histories of the lift and drag coefficients and their power spectra. We observe that the Strouhal number corresponding to the dominant frequency of the lift variation is 0·245 and the mean drag coefficient is 1·53. Experimental results for this flow, quoted in References 1 and 17, report $St = 0{\cdot}21$ and a mean drag coefficient of 1·2. Our computational results overpredict both quantities compared with the experimental results. However, they are in excellent agreement with computational results obtained by other researchers with alternative numerical algorithms and different meshes. Behr *et al.*[18] and Behr[19] computed *Re* 1000 flow past a cylinder using a stabilized velocity–pressure–stress formulation and a mesh with 21,408 quadrilateral elements. They report $St = 0{\cdot}241$ and a mean drag coefficient of 1·53. Rosenfeld and Kwak[20] also report higher values of Strouhal number and mean drag coefficient compared with experimental results. Balachandar and Mittal[21] have reported 2D and 3D simulations for flows past elliptic and circular cylinders at *Re* 525. They have observed that 2D computations tend to overpredict the mean drag coefficients, while results from 3D computations are closer to experimental observations. This suggests that at Reynolds number 1000 the three-dimensional effects are quite significant in the flow and play an important role in determining the overall aerodynamic coefficients.

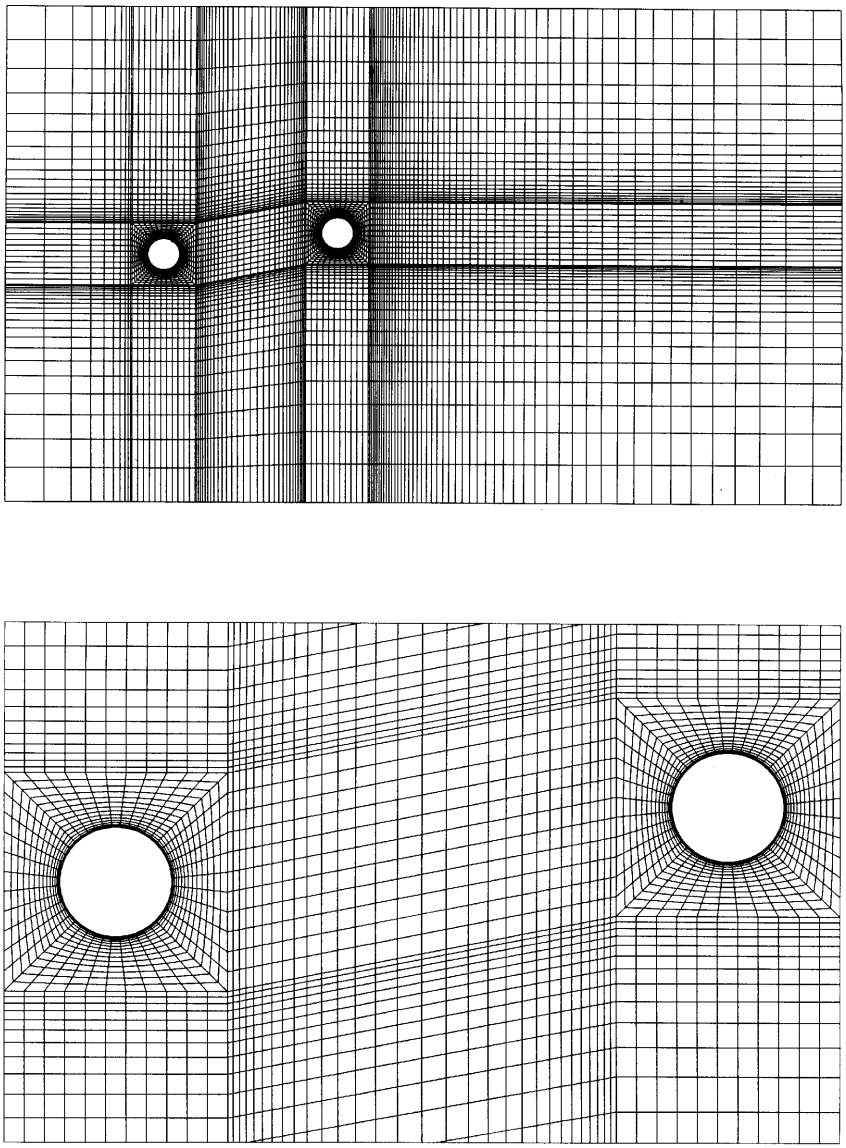

Figure 2. Flow past two cylinders in staggered arrangement, $T/D = 0{\cdot}7$, $P/D = 5{\cdot}5$: finite element mesh with 7260 nodes and 7034 elements

4.2. *Re 100 flow past two cylinders in tandem arrangement: $T/D = 0$, $P/D = 2{\cdot}5$*

It has been reported in the literature[1,2,7] that for this arrangement of the two cylinders there is no distinct vortex shedding behind the upstream cylinder. Our computations lead to the same observation. When the steady state solution is perturbed, after some transience, it converges to the initial steady solution. Shown in Figure 6 are the vorticity, streamfunction and pressure fields for the steady solution. Figure 7 shows the time histories of the lift and drag coefficients for the two cylinders. We observe that the downstream cylinder experiences a 'negative drag', i.e. it feels

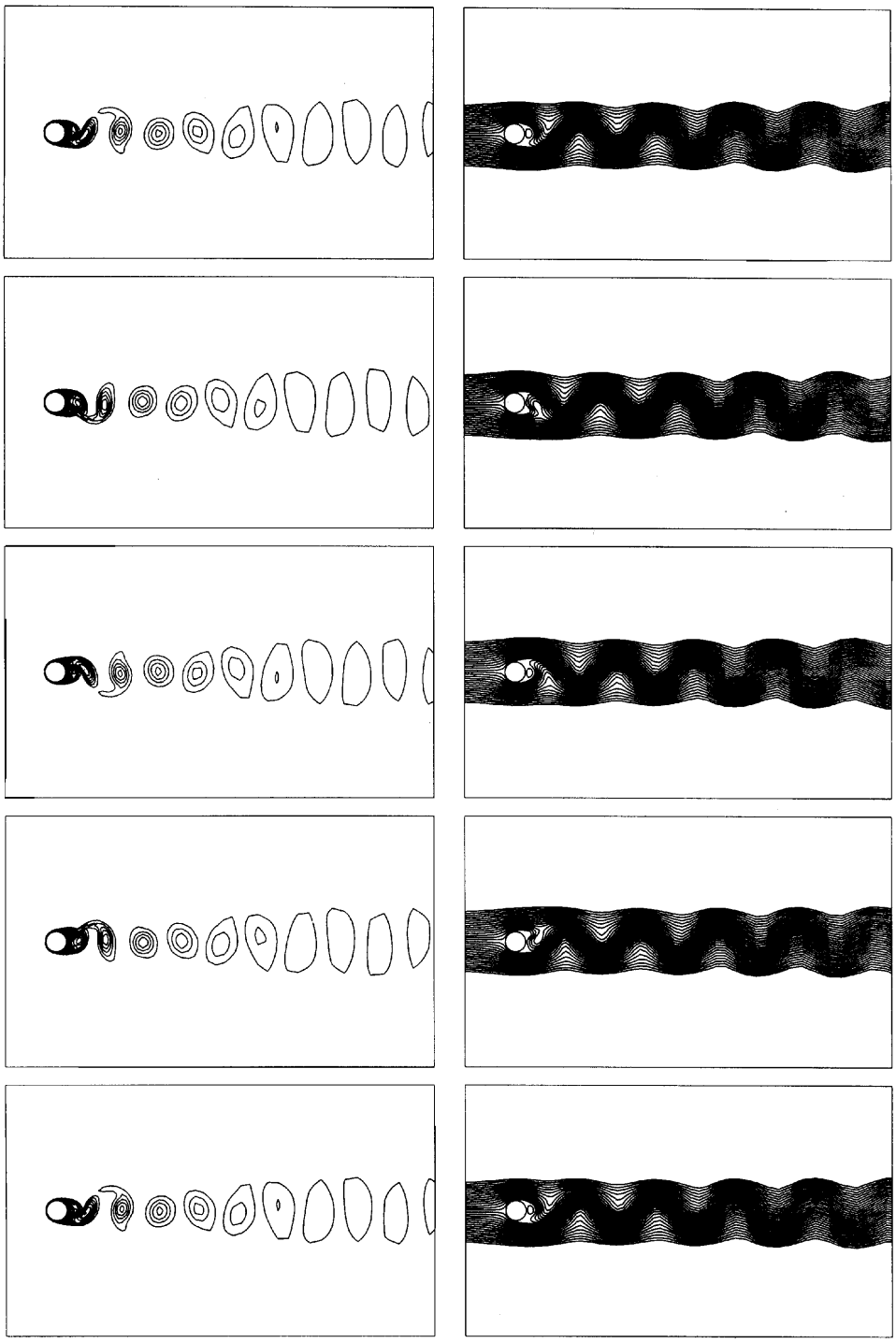

Figure 3. *Re* 1000 flow past a single cylinder: vorticity and streamfunction fields at five instants during one period of lift coefficient

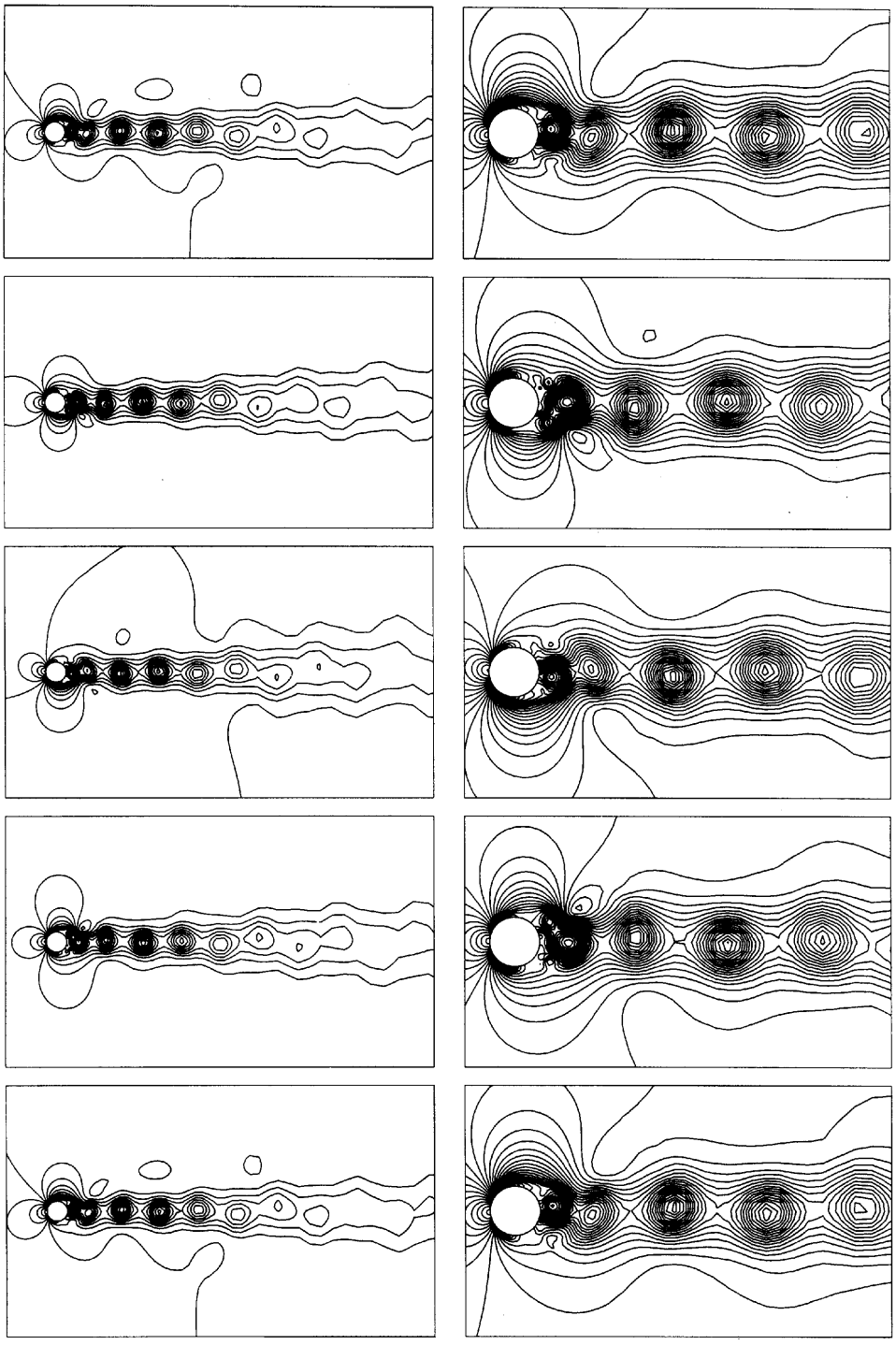

Figure 4. *Re* 1000 flow past a single cylinder: pressure field at five instants during one period of lift coefficient

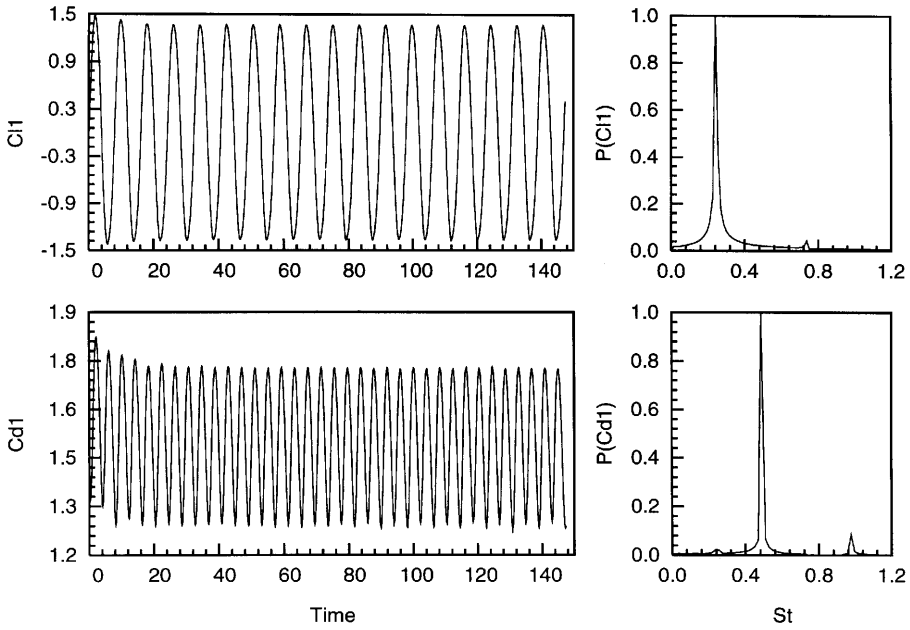

Figure 5. *Re* 1000 flow past a single cylinder: time histories of lift and drag coefficients and their power spectra

attracted towards the upstream cylinder. Additionally, the combined drag of the two cylinders is less than the mean drag for the flow past a single cylinder (results for *Re* 100 flow past a single cylinder have been reported in References 10–13. This observation is consistent with that made by Zdavkovich[1] and Chen.[2] From the flow pictures in Figure 6 we observe that the shear layer that separates from the upstream cylinder reattaches to the downstream one. This renders stability to the shear layer and inhibits the vortex shedding.

4.3. Re 1000 flow past two cylinders in tandem arrangement; $T/D = 0$, $P/D = 2{\cdot}5$

The flow at *Re* 100 is used as an initial condition to compute the flow at *Re* 1000. At *Re* 1000 our computations reveal an unsteady flow. Shown in Figure 8 are the vorticity fields for the solution in the initial stages of the simulation. As a result of the increased Reynolds number, the shear layer develops instability. It is interesting to observe that first the asymmetry in the flow develops downstream and then it propagates upstream. Figures 9 and 10 show the vorticity, streamfunction and pressure fields during one cycle of the lift coefficient for the upstream cylinder for the nearly periodic solution. From these figures we observe that there is a very complex interaction between the vortices shed by the upstream cylinder and the downstream cylinder. A counter-clockwise rotating vortex from the first cylinder hits the second one (rows 1–3 in the flow pictures) more towards its lower surface. At this point the downstream cylinder is about to shed a clockwise rotating vortex from its upper surface. While this clockwise rotating vortex is shed from the upper surface of the downstream cylinder, the above-mentioned counter-clockwise rotating vortex glides along the upper surface of the second cylinder and interacts with another counter-clockwise rotating vortex forming in the wake of the second cylinder. The process is repeated for the counter-rotating set of vortices in the second half of the shedding cycle. The shedding from the two cylinders is almost antiphase; that is, as the first cylinder sheds a vortex from the upper surface, the second one sheds a counter-rotating one from the lower surface. The wake behind the downstream cylinder consists of two rows of staggered vortices

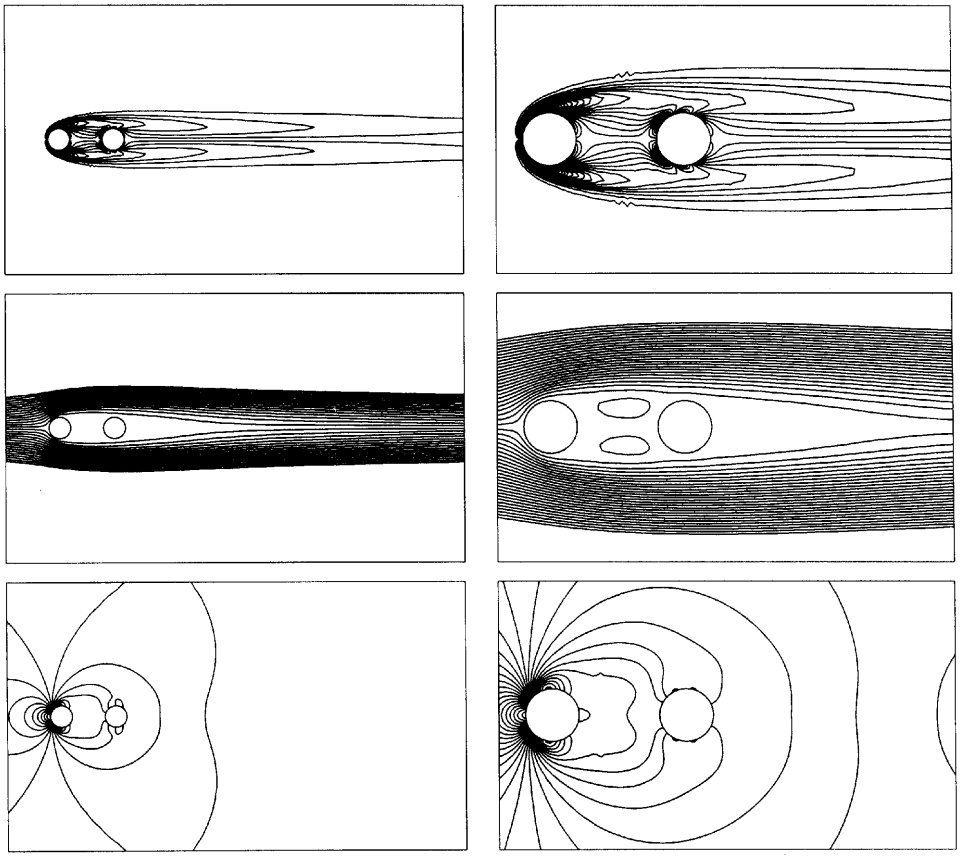

Figure 6. *Re* 100 flow past two cylinders in tandem arrangement, $T/D = 0, P/D = 2{\cdot}5$: vorticity, streamfunction and pressure fields for steady solution

of alternate signs. The lateral width of the wake is significantly larger than that for the single-cylinder case at the same Reynolds number. Figure 11 shows the time histories of the lift and drag coefficients and their power spectra for the two cylinders. Our computed results are quite consistent with observations made by other researchers based on laboratory experiments.[1,2,7] We observe that, compared with the single-cylinder case, the Strouhal number for this case is quite low. As a result of the interference between the two cylinders, compared with the single-cylinder case, there is a decrease in the mean drag coefficient for both cylinders. It has been reported that there is no distinct vortex shedding behind the upstream cylinder till the distance between the centres of the two cylinders is less then a certain critical spacing. Kiya *et al.*[7] report that beyond $P/D = 3$ the vortex shedding suddenly becomes distinct and its frequency soon reaches the value found behind the single cylinder. Other researchers have reported this critical spacing to be $P/D = 3{\cdot}8$. Perhaps the critical spacing is very sensitive to the Reynolds number and to the experimental set-up and that is why our solutions show a vortex shedding behind the upstream cylinder. Kiya *et al.*[8] conducted experiments involving two cylinders in tandem with $P/D = 3{\cdot}47$. They observed two distinct flow patterns which switch randomly in time. The Reynolds numbers in their experiments were in the range $(2{\cdot}0–3{\cdot}0) \times 10^4$. A detailed numerical study is needed to understand this interesting phenomenon.

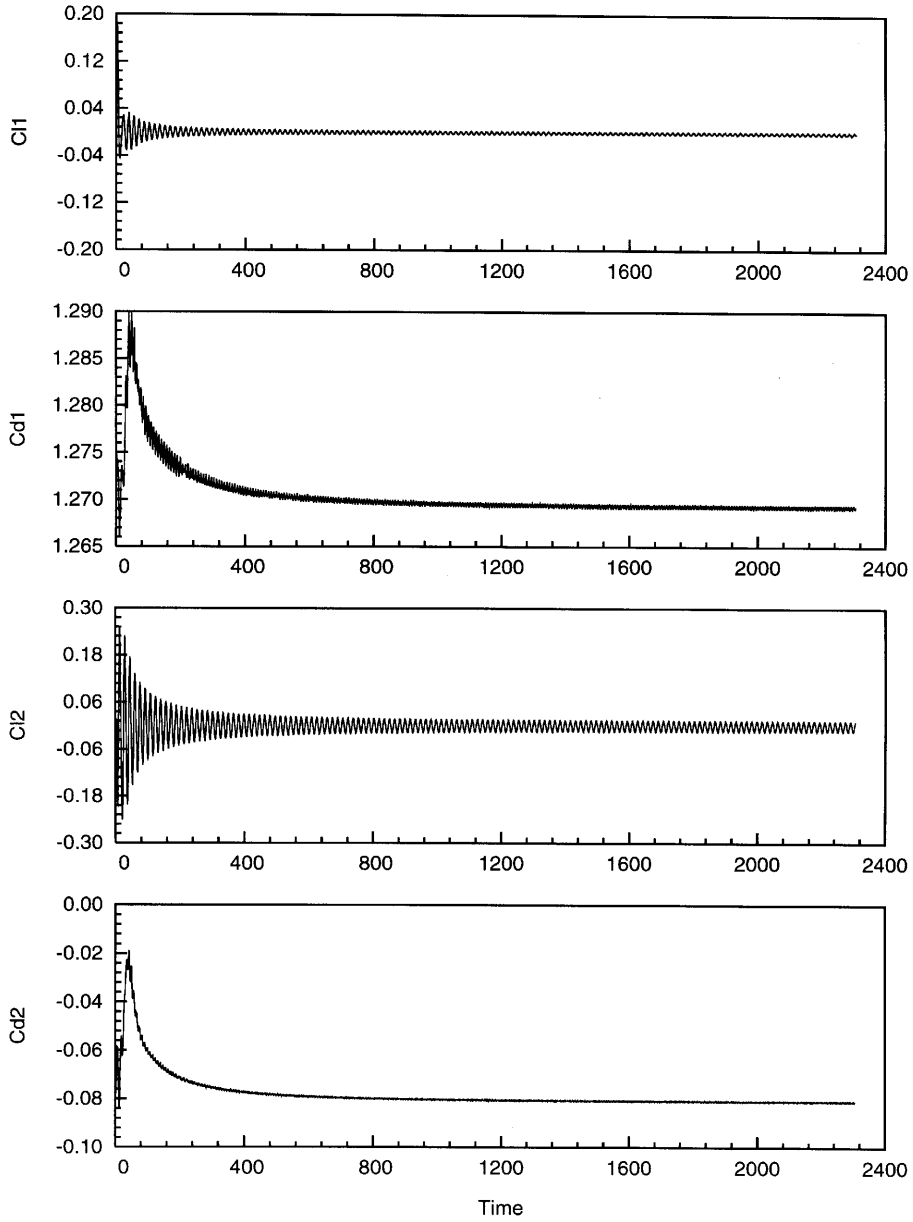

Figure 7. *Re* 100 flow past two cylinders in tandem arrangement, $T/D = 0, P/D = 2{\cdot}5$: time histories of lift and drag coefficients

4.4. Re 100 flow past two cylinders in tandem arrangement $T/D = 0$, $P/D = 5{\cdot}5$

When the spacing between the two tandem cylinders is increased, our computations indicate an unsteady solution for $Re = 100$. Figures 12 and 13 show the vorticity, streamfunction and pressure fields during one cycle of the lift coefficient for the upstream cylinder for the periodic solution. Qualitatively, the flow is quite similar to the Re 1000 case with $T/D = 0$ and $P/D = 2{\cdot}5$, although

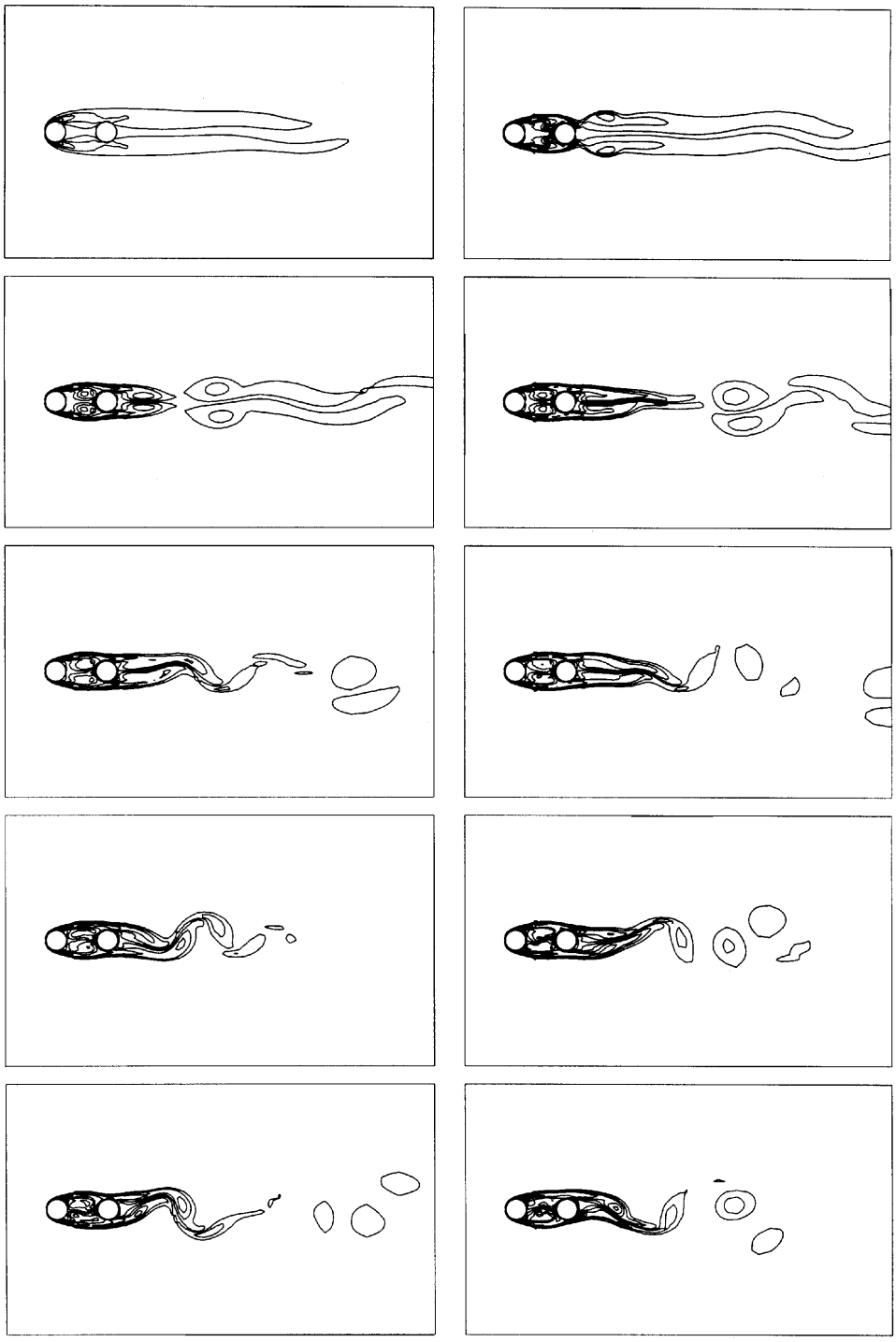

Figure 8. *Re* 1000 flow past two cylinders in tandem arrangement, $T/D = 0$, $P/D = 2{\cdot}5$: vorticity field at $t = 0$, 10, 20, 30, 40, 50, 60, 70, 80 and 90 (left to right and then top to bottom)

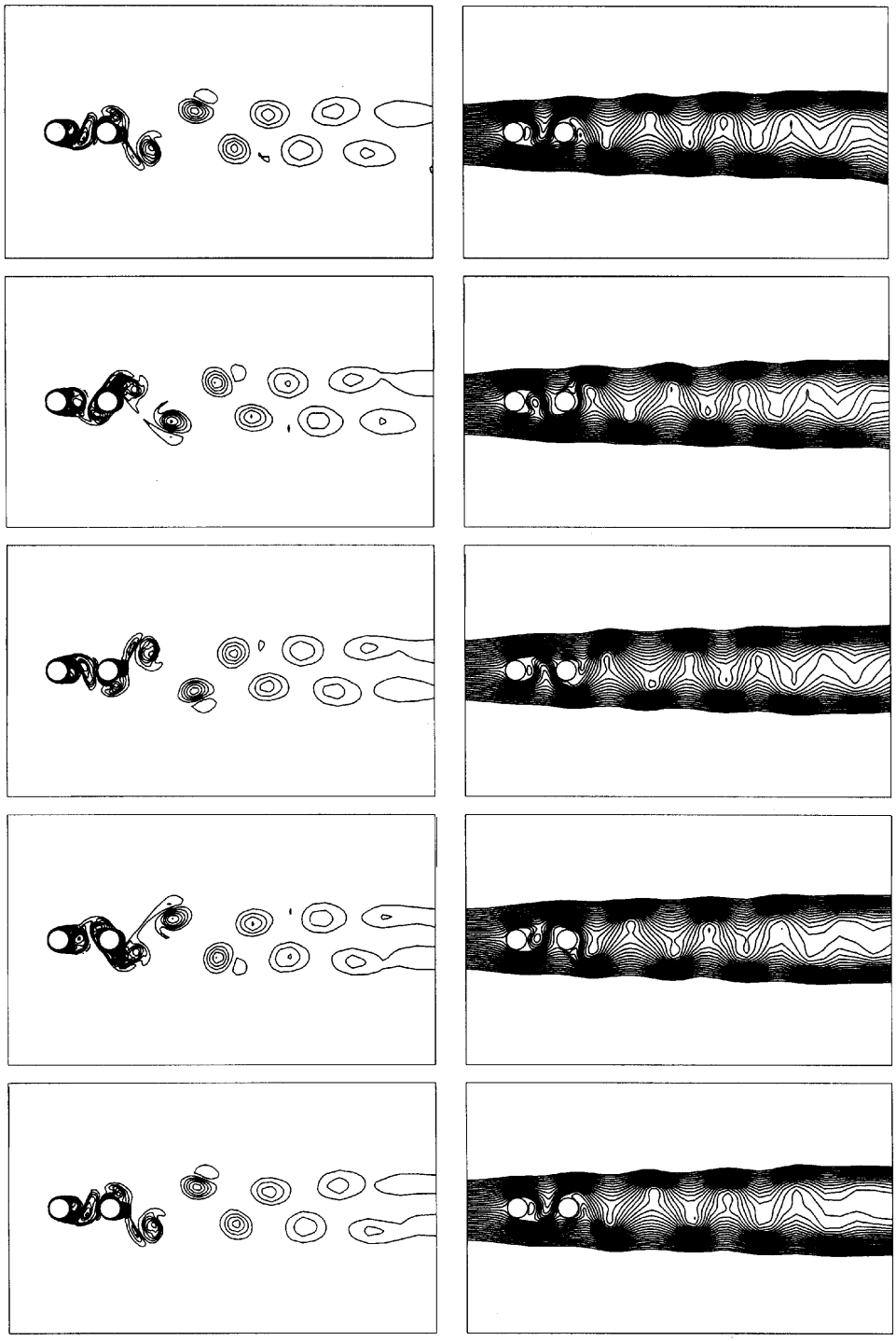

Figure 9. *Re* 1000 flow past two cylinders in tandem arrangement, $T/D = 0, P/D = 2{\cdot}5$: vorticity and streamfunction fields at five instants during one period of lift coefficient for upstream cylinder

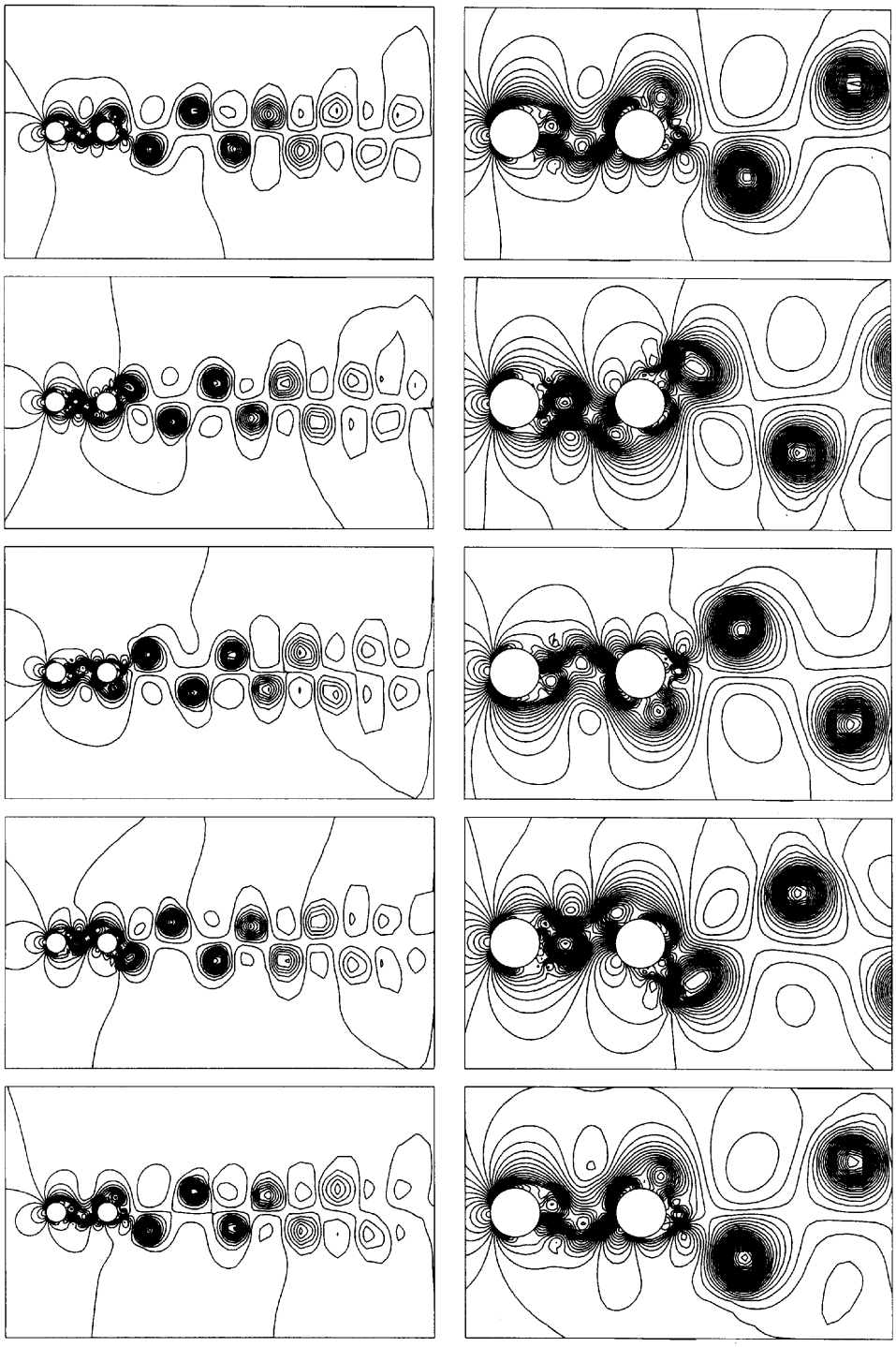

Figure 10. *Re* 1000 flow past two cylinders in tandem arrangement, $T/D = 0, P/D = 2{\cdot}5$: pressure field at five instants during one period of lift coefficient for upstream cylinder

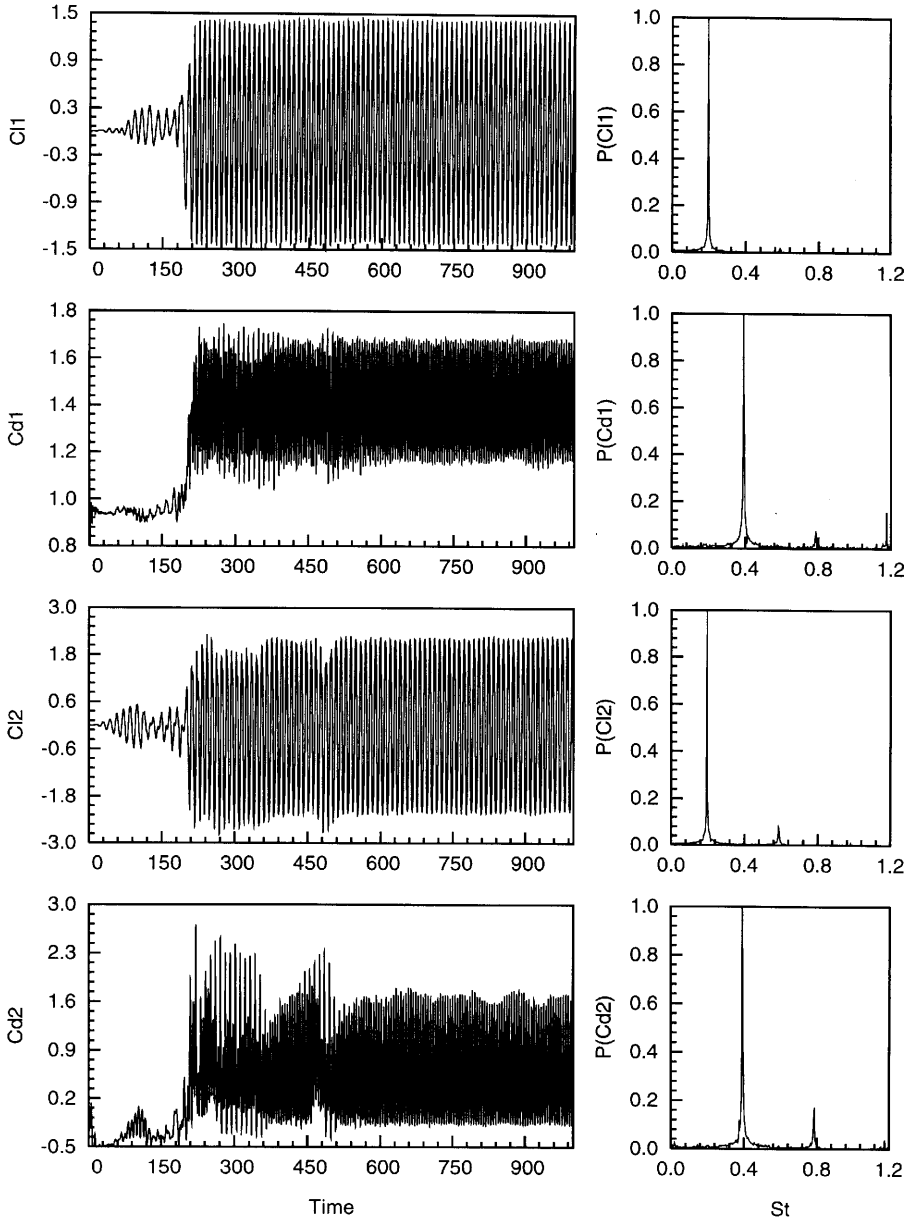

Figure 11. *Re* 1000 flow past two cylinders in tandem arrangement, $T/D = 0, P/D = 2{\cdot}5$: time histories of lift and drag coefficients and their power spectra

the wake is much more organized in the present case. The vortex shedding from the two cylinders is almost antiphase; that is, as the first cylinder sheds a vortex from the upper surface, the second one sheds a counter-rotating one from the lower surface. Also noticeable in the flow pictures is the rather violent movement of the stagnation point for the rear cylinder. Figure 14 shows the time histories of the lift and drag coefficients and their power spectra for the two cylinders. We observe that the Strouhal number for both cylinders is very close to that for a single cylinder. The drag and lift

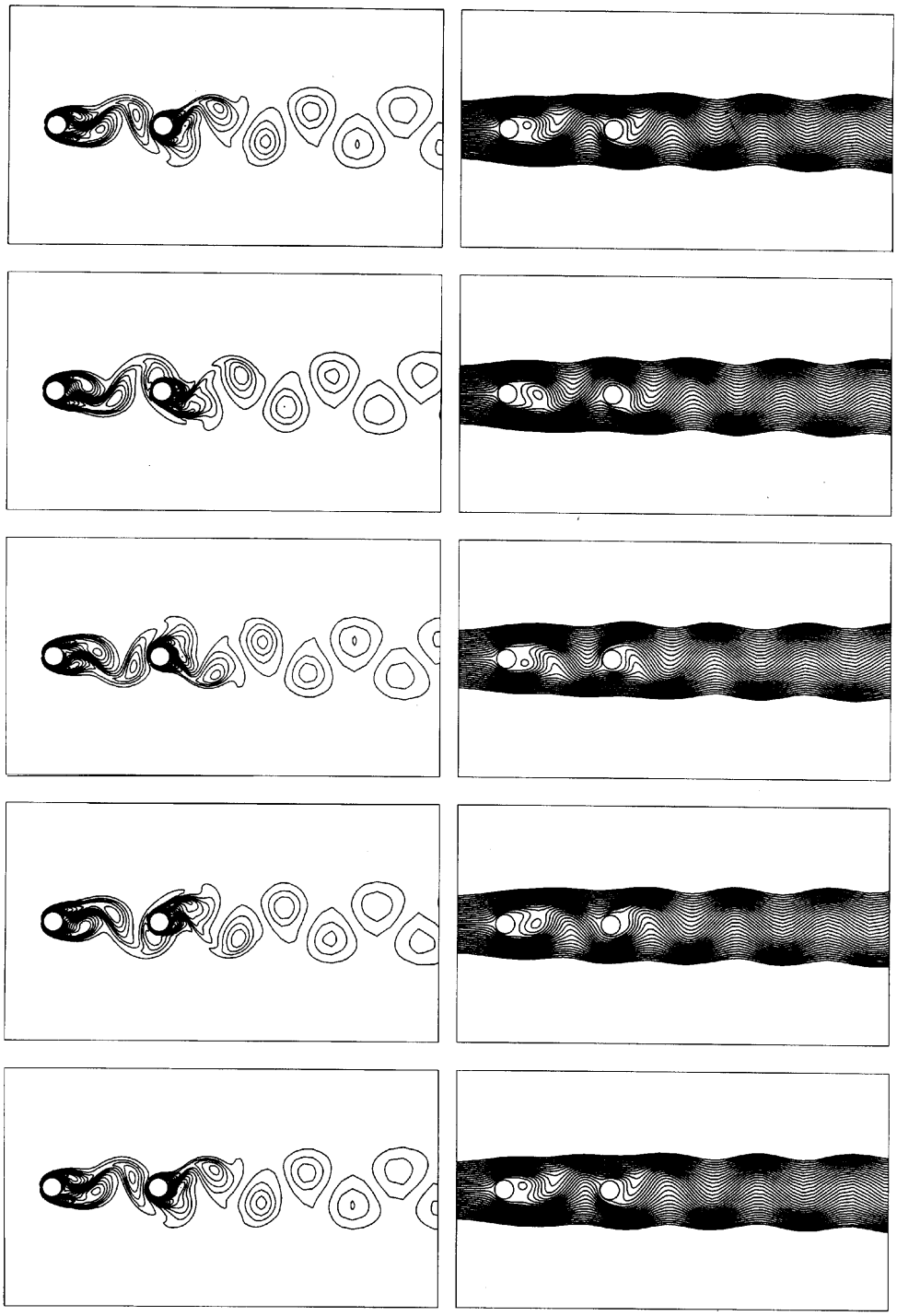

Figure 12. *Re* 100 flow past two cylinders in tandem arrangement, $T/D = 0, P/D = 5{\cdot}5$: vorticity and streamfunction fields at five instants during one period of lift coefficient for upstream cylinder

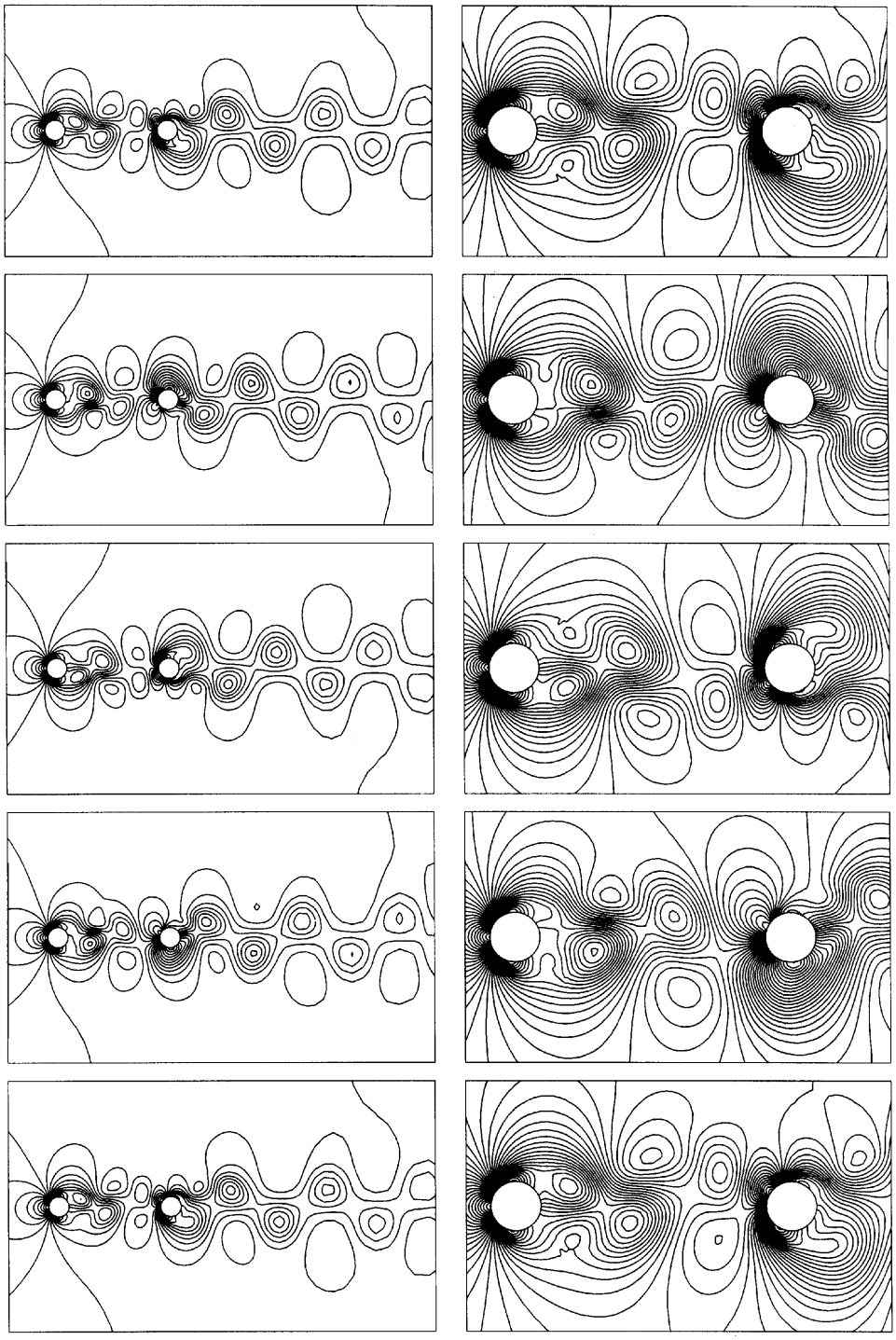

Figure 13. *Re* 100 flow past two cylinders in tandem arrangement, $T/D = 0, P/D = 5{\cdot}5$: pressure field at five instants during one period of lift coefficient for upstream cylinder

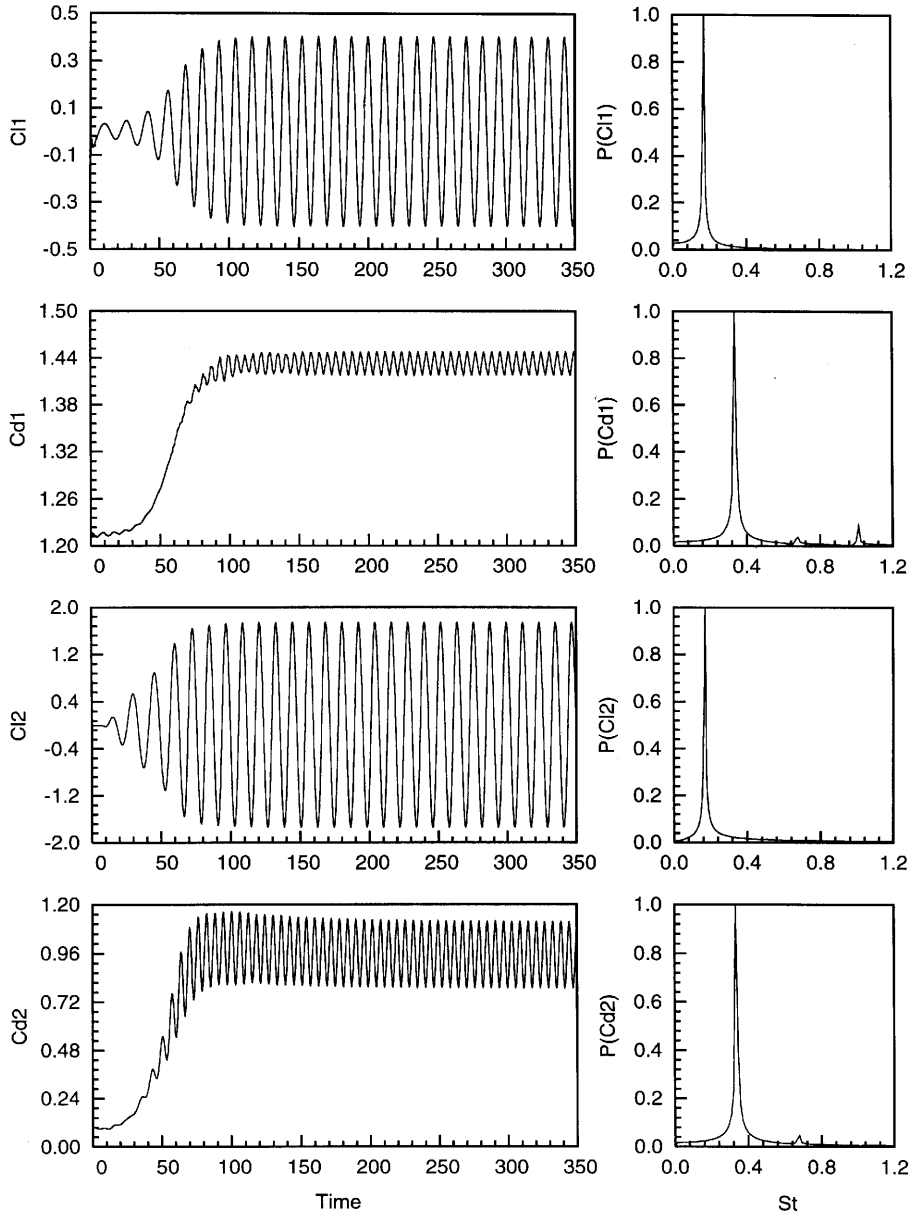

Figure 14. *Re* 100 flow past two cylinders in tandem arrangement, $T/D = 0, P/D = 5{\cdot}5$: time histories of lift and drag coefficient and their power spectra

coefficients for the upstream cylinder are quite comparable with the values for a single cylinder. As expected, since the downstream cylinder is directly in the wake of the first cylinder, the aerodynamic coefficients are affected quite significantly. These computations are carried out with a mesh consisting of 8753 nodes and 8504 quadrilateral elements.

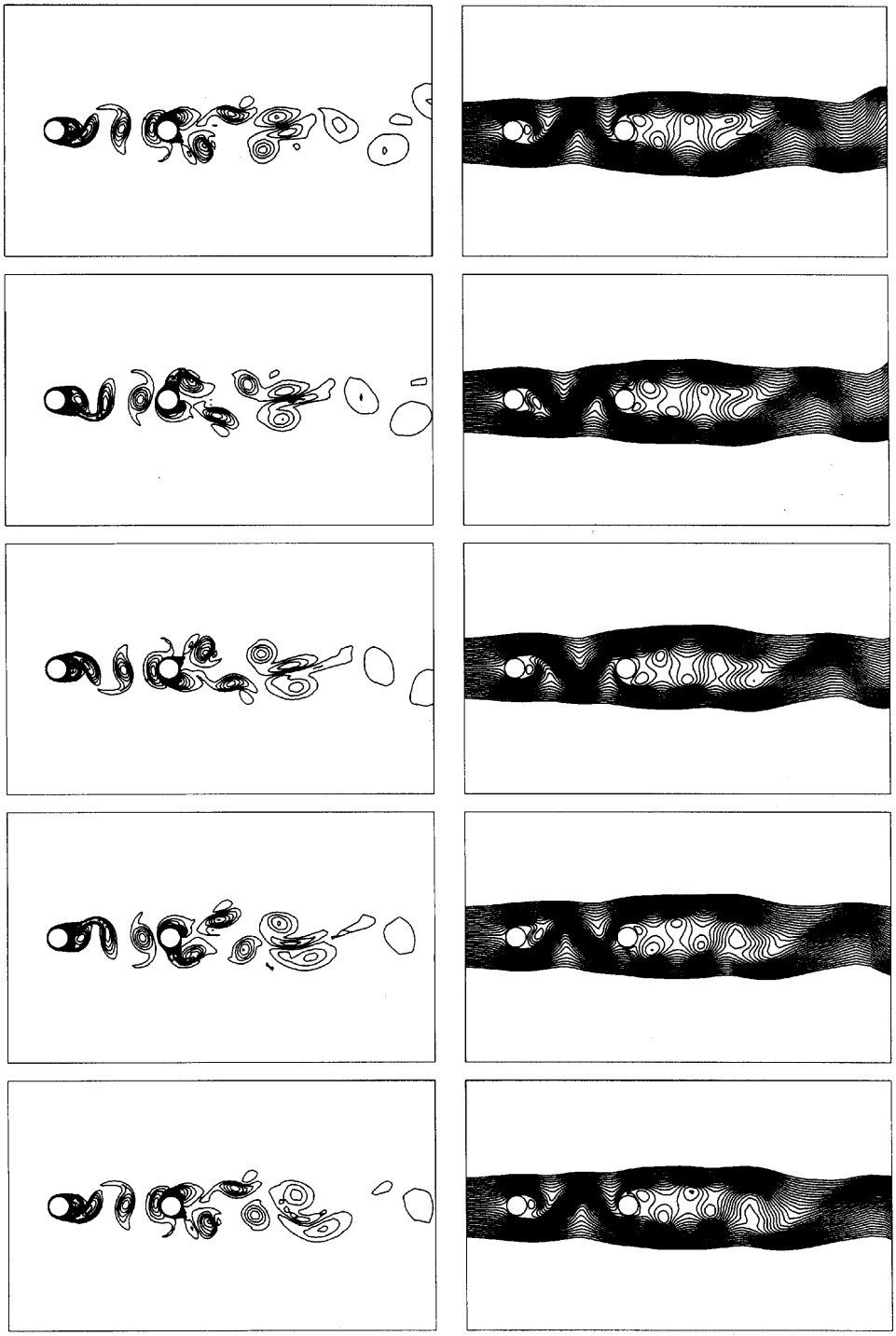

Figure 15. *Re* 1000 flow past two cylinders in tandem arrangement, $T/D = 0$, $P/D = 5{\cdot}5$: vorticity and streamfunction fields at five instants during one period of lift coefficient for upstream cylinder

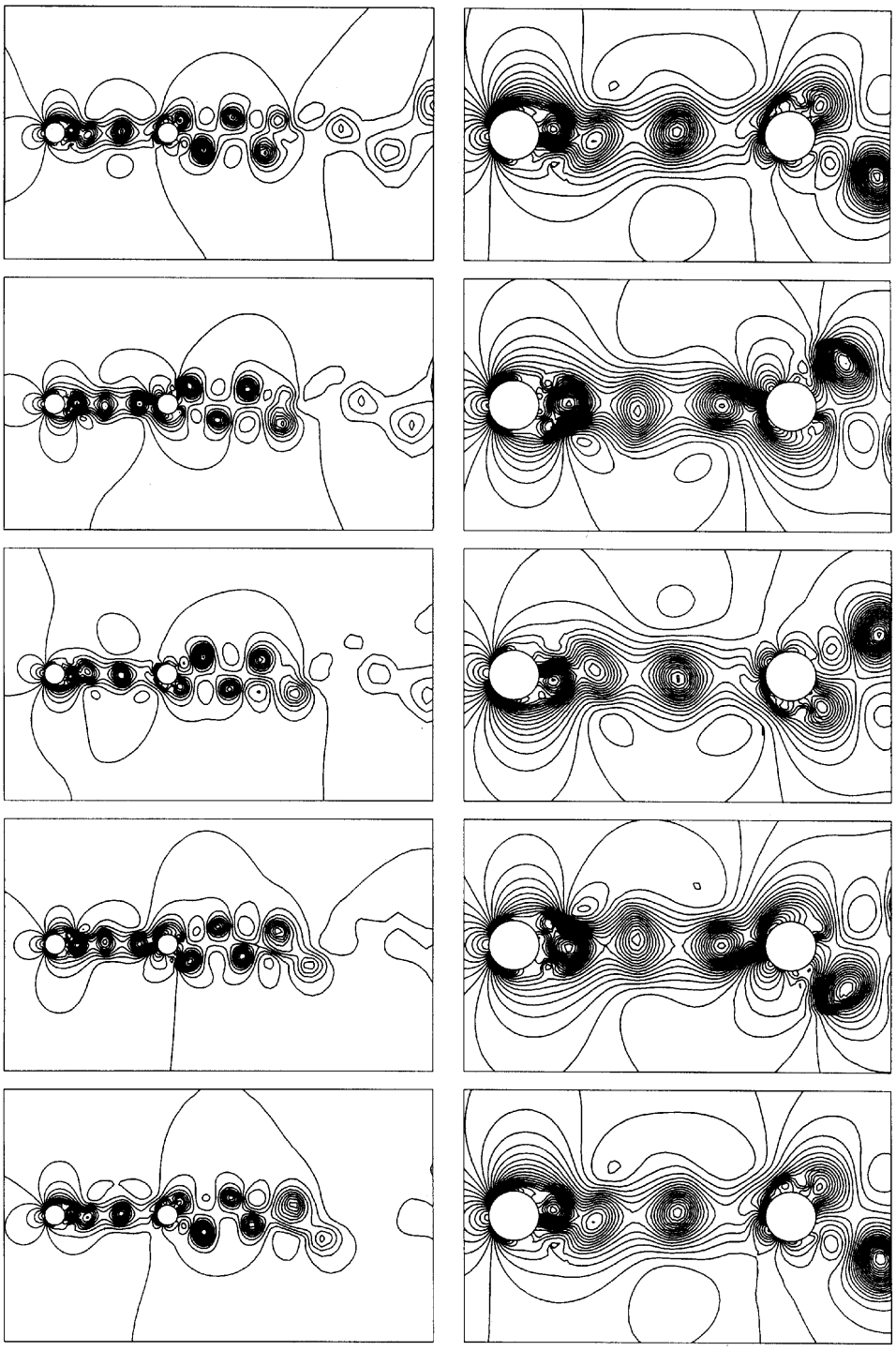

Figure 16. *Re* 1000 flow past two cylinders in tandem arrangement, $T/D = 0$, $P/D = 5{\cdot}5$: pressure field at five instants during one period of lift coefficient for upstream cylinder

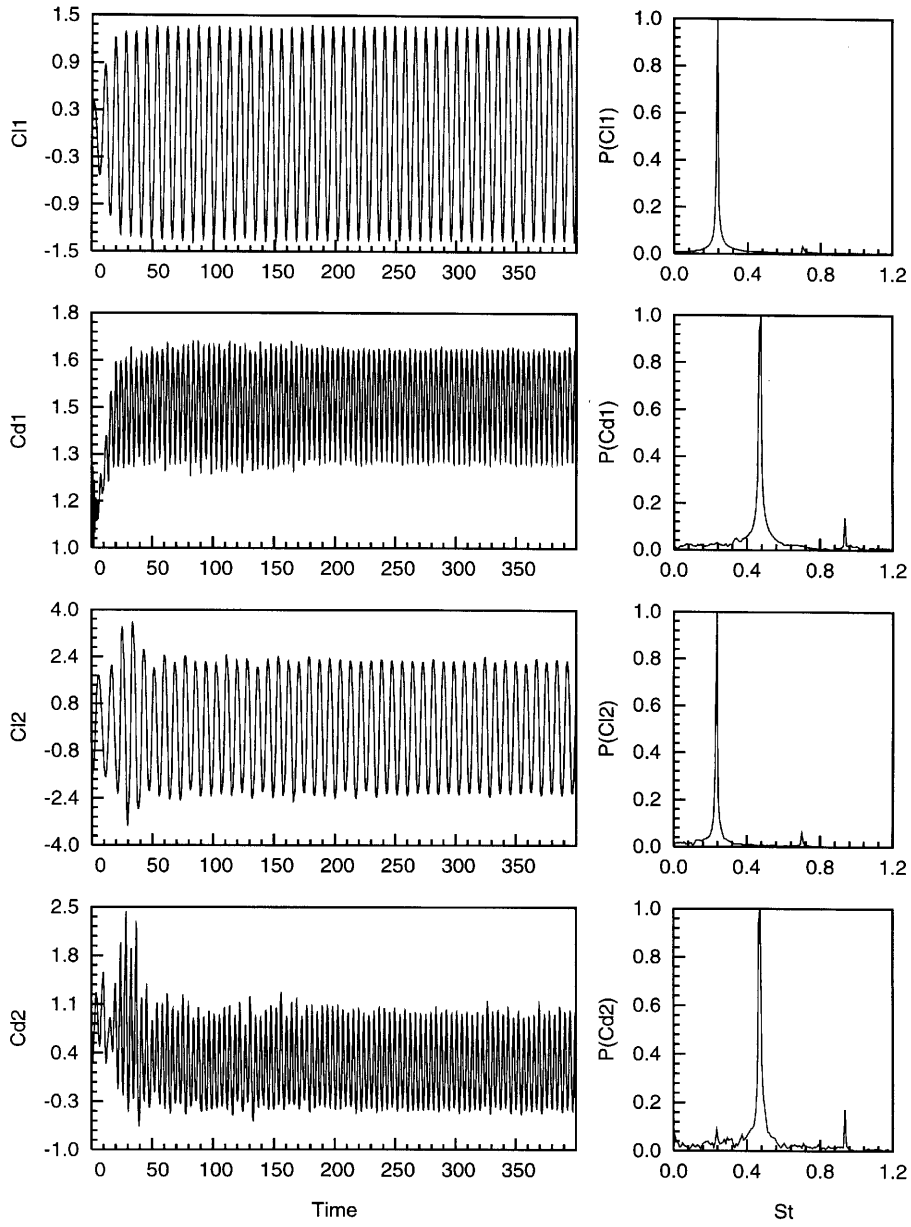

Figure 17. *Re* 1000 flow past two cylinders in tandem arrangement, $T/D = 0, P/D = 5{\cdot}5$: time histories of lift and drag coefficients and their power spectra

4.5. Re 1000 flow past two cylinders in tandem arrangement; $T/D = 0$, $P/D = 5{\cdot}5$

For this case, Figures 15 and 16 show the vorticity, streamfunction and pressure fields during one cycle of the lift coefficient for the upstream cylinder when the solution attains an almost temporally periodic state. From the flow pictures we observe that, as in the previous case, the vortex shedding from the two cylinders is almost antiphase. It can also be observed that although the flow structures in

the near wake of the two cylinders are temporally periodic, the flow structures in the far wake are not. This can be attributed to the strong interaction between the vortices shed from the two cylinders. The wake behind the rear cylinder is not as organized as the one at *Re* 100. It can be observed that downstream of the second cylinder the vortices bunch up in groups of two or three and their motions are strongly affected by the induced velocities due to the surrounding vortices. Figure 17 shows the time histories of the lift and drag coefficients and their power spectra for the two cylinders. From this picture it can be seen that the upstream cylinder does not seem to be affected too much by the downstream one and behaves almost like a single cylinder. This, however, cannot be said about the downstream cylinder, which experiences large unsteady forces because of being in the wake of the first one. This has implications in the context of engineering structures, e.g. a set of chimneys or control towers, where the downstream body experiences very large unsteady forces that may lead to large-amplitude oscillations.

4.6. Re 100 flow past two cylinders in staggered arrangement; $T/D = 0{\cdot}7$, $P/D = 5{\cdot}5$

The staggered arrangement of cylinders is the one that is most likely to occur in an engineering situation, e.g. in heat exchangers and other cooling systems involving tube bundles. Experimental investigations of such arrangements have been reported by various researchers in the past.[1,2,7] Numerical simulations of flow past periodic arrays of cylinders at *Re* 100 were reported by Johnson *et al.*[9]

The present computations are carried out with a mesh that consists of 7260 nodes and 7054 elements. A view of the mesh is shown in Figure 2, Shown in Figures 18 and 19 are the vorticity, streamfunction and pressure fields during one cycle of the lift coefficient for the upstream cylinder when the solution attains an almost temporally periodic state. When we compare these flow pictures with those for flows past cylinders in tandem, we observe very significant differences. Unlike the previous cases, this time the vortex shedding from the two cylinders is almost synchromized, e.g. both cylinders shed vortices from their upper surfaces at approximately the same time. The counterclockwise rotating vortices that are shed from the lower surface of the upstream cylinder pass below the downstream cylinder and interact with the counter-clockwise rotating vertex shed from its lower surface. The two coalesce downstream and one can observe a row of counter-clockwise rotating vortices that are elongated along the flow direction. The clockwise rotating vortices that are shed from the upper surface of the upstream cylinder hit the rear one and split into two. The one that glides along the lower surface gets diffused quite soon, while the one that moves towards the upper surface of the downstream cylinder interacts with its clockwise rotating vortex. This interaction produces a stronger vortex that is shed from the upper surface of the second cylinder and one can observe a row of such vortices in the wake. Figure 20 shows the time histories of the lift and drag coefficients and their power spectra for the two cylinders. Compared with the other cases, the power spectrum of the drag coefficient for the first cylinder contains components at additional frequencies. It is quite interesting to note that these components do not appear in the lift coefficient. This could be attributed to the inherent geometric asymmetry of the problem. It is well known that for the flow past an isolated cylinder the drag coefficient varies at twice the temporal frequency of the variation in the lift coefficient. Each cycle of the variation in the drag coefficient corresponds to a vortex shed from either the upper or lower surface of the cylinder. In the present case the vortices shed from the lower and upper surfaces of the two cylinders meet a different fate owing to the inherent geometric asymmetry in the problem. Consequently, one observes a difference in the drag force felt by the cylinder during vortex-shedding cycles from its upper and lower surfaces. As a result of this asymmetry, the mean value of the lift coefficient over a cycle of vortex shedding is non-zero.

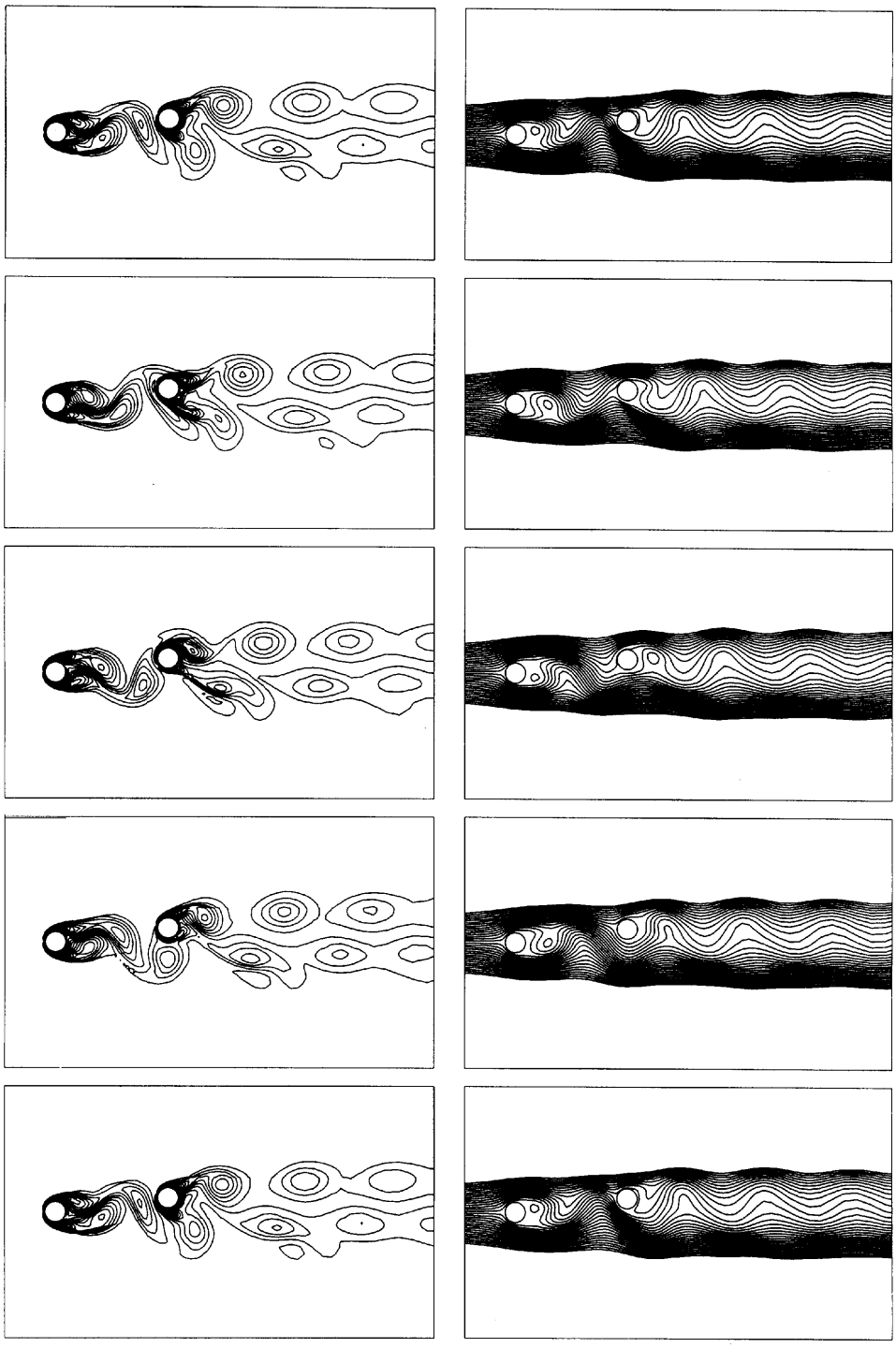

Figure 18. *Re* 100 flow past two cylinders in staggered arrangement, $T/D = 0{\cdot}7$, $P/D = 5{\cdot}5$: vorticity and streamfunction fields at five instants during one period of lift coefficient for upstream cylinder

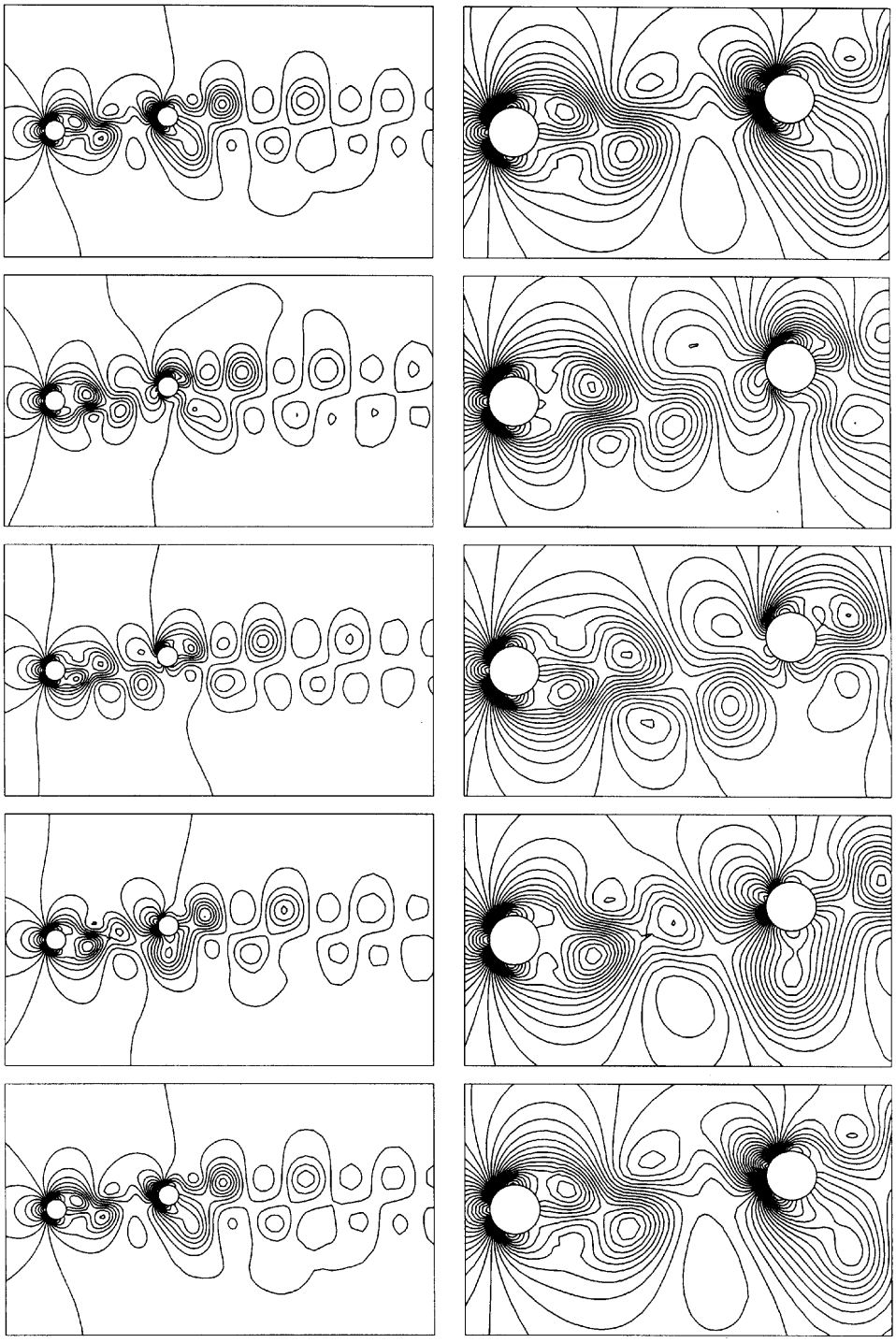

Figure 19. *Re* 100 flow past two cylinders in staggered arrangement, $T/D = 0{\cdot}7$, $P/D = 5{\cdot}5$: pressure field at five instants during one period of lift coefficient for upstream cylinder

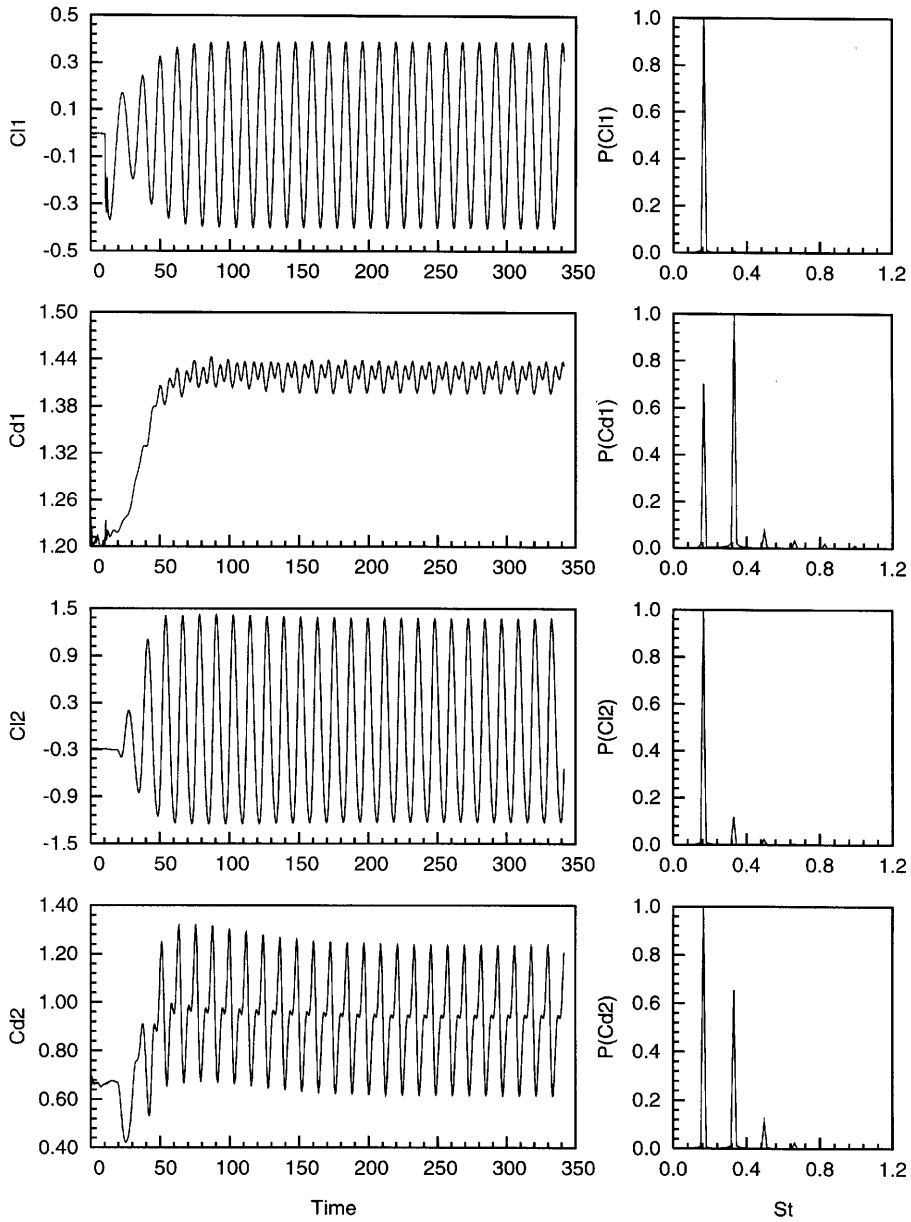

Figure 20. *Re* 100 flow past two cylinders in staggered arrangement, $T/D = 0{\cdot}7, P/D = 5{\cdot}5$: time histories of lift and drag coefficients and their power spectra

4.7. Re 1000 flow past two cylinders in staggered arrangment; $T/D = 0{\cdot}7$, $P/D = 5{\cdot}5$

Figures 21 and 22 show the vorticity, streamfunction and pressure fields during one cycle of the lift coefficient for the upstream cylinder when the solution attains an almost temporally periodic state. We observe that this flow is quite different from that of Reynolds number 100. In contrast with the flow at *Re* 100, the vortex shedding from the two cylinders in the present case is almost antiphase.

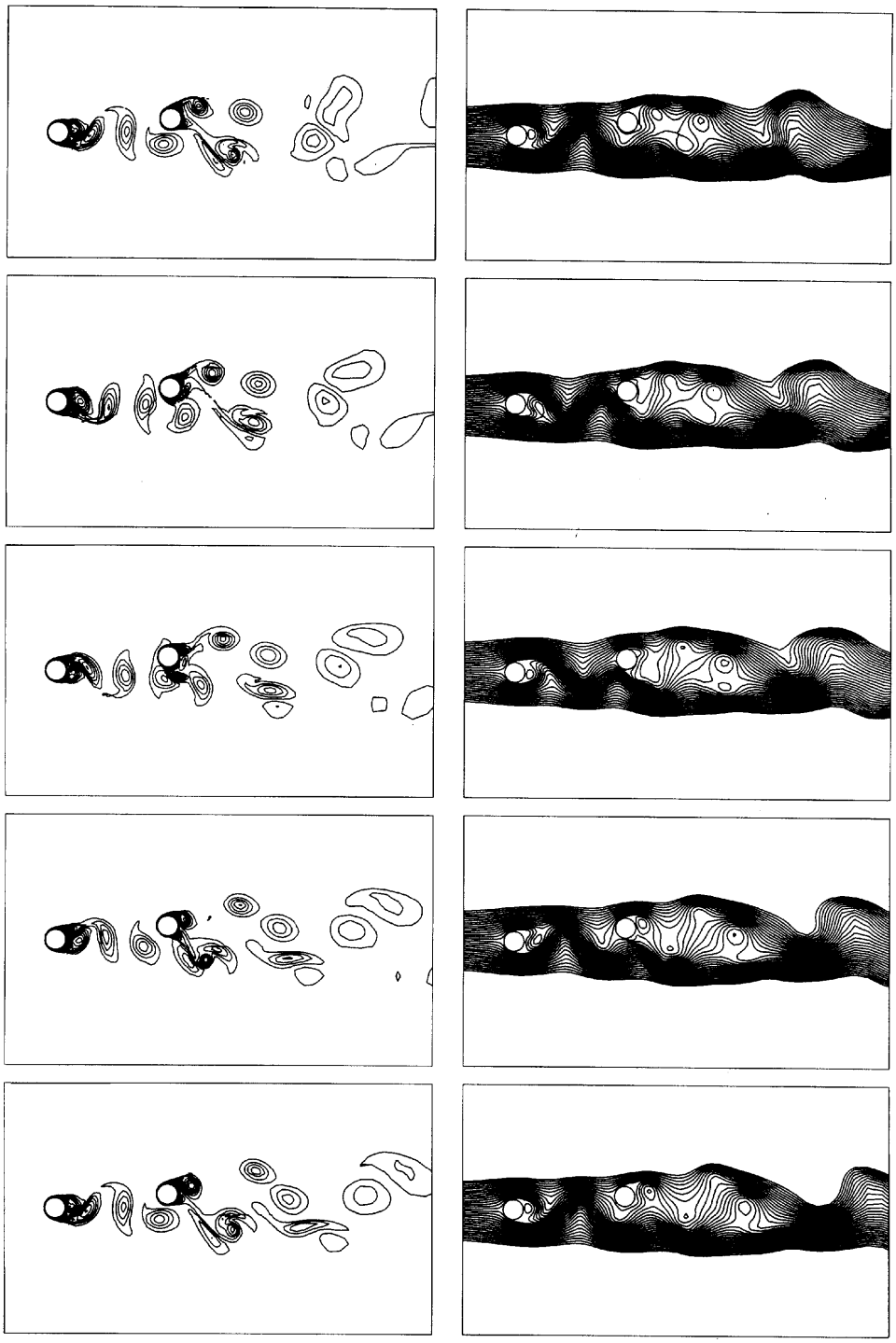

Figure 21. *Re* 1000 flow past two cylinders in staggered arrangement, $T/D = 0{\cdot}7, P/D = 5{\cdot}5$: vorticity and streamfunction fields at five instants during one period of lift coefficient for upstream cylinder

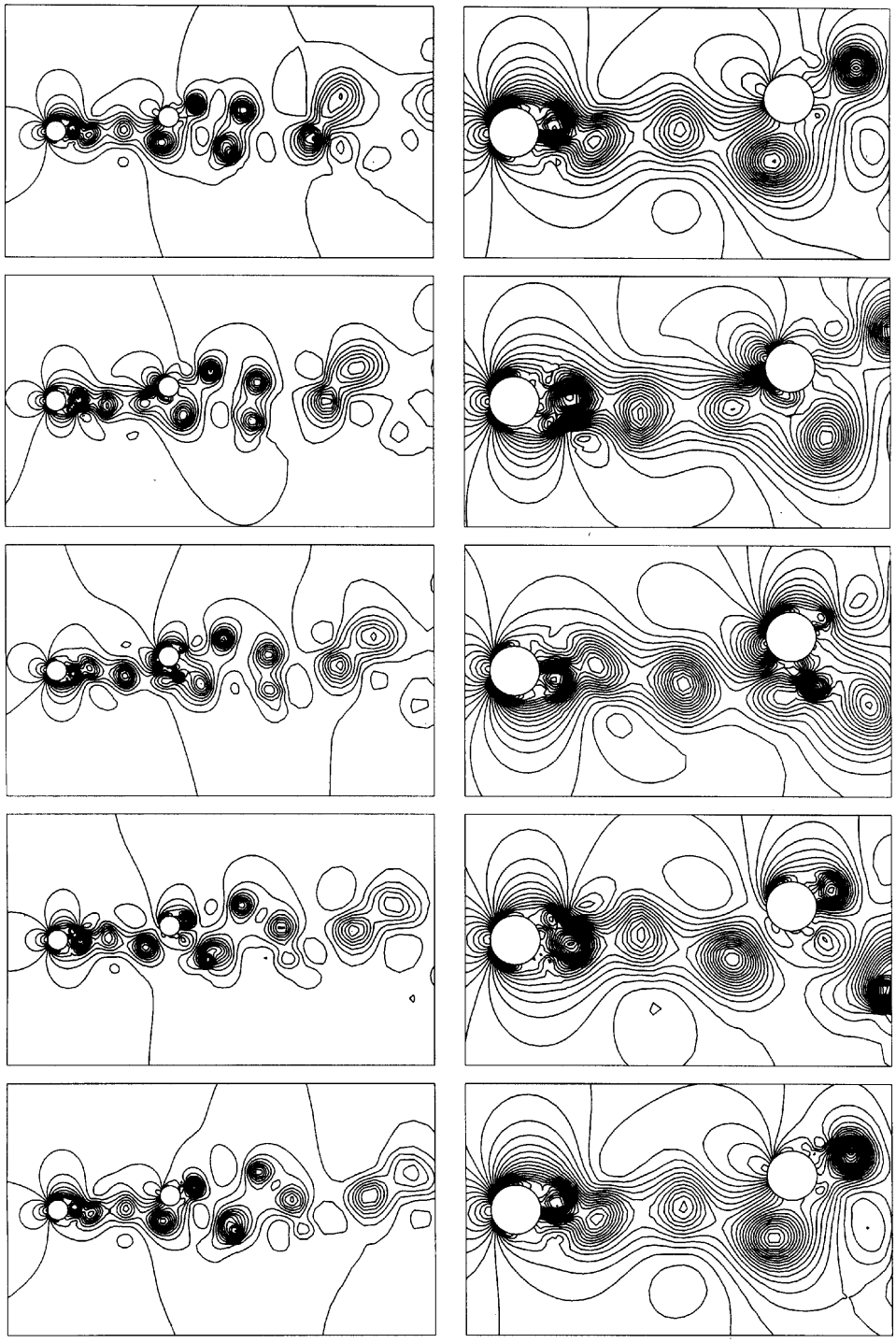

Figure 22. *Re* 1000 flow past two cylinders in staggered arrangement, $T/D = 0{\cdot}7$, $P/D = 5{\cdot}5$: pressure field at five instants during one period of lift coefficient for upstream cylinder

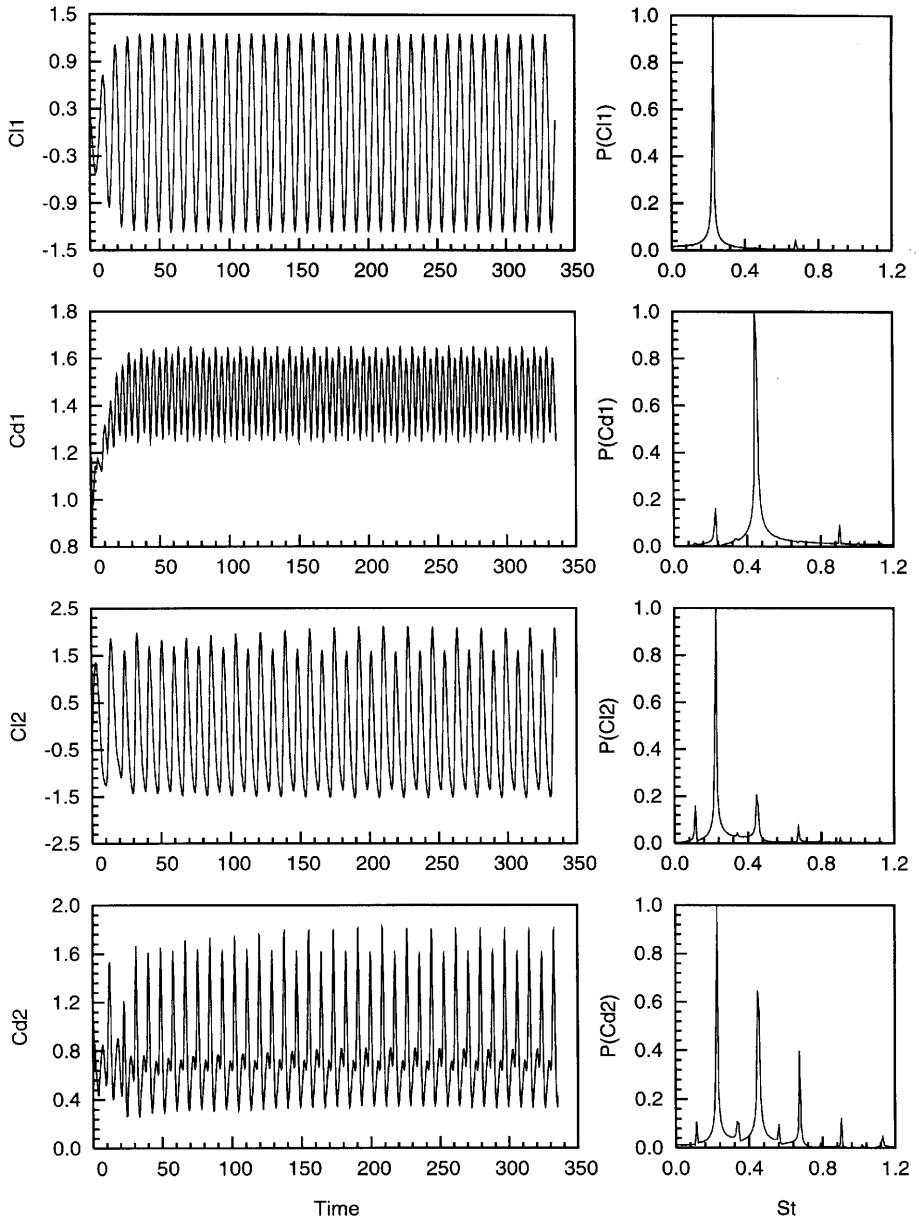

Figure 23. *Re 1000* flow past two cylinders in staggered arrangement, $T/D = 0{\cdot}7$, $P/D = 5{\cdot}5$: time histories of lift and drag coefficients and their power spectra

The vortices that are shed from the upper and lower surfaces of the upstream cylinders pass below the lower surface of the downstream cylinder. Their interaction with the upper surface of the downstream cylinder is quite insignificant compared with that in the previous cases. Both the clockwise and counter-clockwise rotating vortices shed from the first cylinder interact quite strongly with the counter-clockwise rotating vortex shed from the lower surface of the second cylinder. These vortices form a 'triplet' that 'tumbles' along as they advect downstream and finally coalesce. They also

interact with the clockwise rotating vortices that are shed from the upper surface of the rear cylinder. Figure 23 shows the time histories of the lift and drag coefficients and their power spectra for the two cylinders. As a result of this complex interaction between the vortices shed from the two cylinders, the dominant frequency in the time history of the drag coefficient for the second cylinder is the same as that for the lift coefficient. Our observations from the computed results are quite consistent with those from laboratory experiments by other researchers.[1,2,7] For example, for the present arrangement the experimental results suggest a slightly lower Strouhal number for the vortex shedding, a negative value of the mean lift coefficient and a lower value of the mean drag coefficient for the second cylinder compared with the single-cylinder case.

5. CONCLUSIONS

A numerical study has been carried out to study the interference effects in flows involving a pair of cylinders in in-line and staggered arrangements at *Re* 100 and 1000. Results for the unsteady flow past a single cylinder at *Re* 1000 have also been presented. A summary of the aerodynamic coefficients for the computed flows is given in Table I.

For the unsteady flows the Strouhal numbers reported in the table correspond to the dominant frequency in the time history of the lift coefficients, while the mean values of the drag and lift coefficients are calculated by integration of data for 10 vortex-shedding cycles of the periodic solution.

Our results for the flow past a single cylinder at *Re* 1000 compare quite well with computational results from other researchers. However, compared with experimental observations, the mean drag coefficient and the Strouhal number are overpredicted. This can perhaps be attributed to the three-dimensional effects in the flow field. The results for flows past two cylinders show good qualitative agreement with those from experiments conducted by other researchers. The flows at *Re* 100 and 1000 exhibit very significant qualitative differences. This points to the fact that the flows involving

Table I. Summary of aerodynamic data for flows past cylinders

	Case 1 ⊕	Case 2 $T/D = 0, P/D = 2{\cdot}5$ ⊕ ⊕ ⟷ $2{\cdot}5D$		Case 3 $T/D = 0, P/D = 5{\cdot}5$ ⊕ ⊕ ⟷ $5{\cdot}5D$		Case 4 $T/D = 0{\cdot}7, P/D = 5{\cdot}5$ ⊕ $0{\cdot}7D$↕ ⊕ ⟷ $5{\cdot}5D$	
		Cylinder 1	Cylinder 2	Cylinder 1	Cylinder 2	Cylinder 1	Cylinder 2
Re 100							
Mean C_D	1.386	1.271	−0.075	1.433	0.952	1.419	0.919
Amplitude C_D	0.011	—	—	0.015	0.164	0.020	0.312
Mean C_L	0.0	0.0	0.0	0.0	0.0	−0.006	−0.045
Amplitude C_L	0.370	—	—	0.403	1.741	0.396	1.300
Strouhal no.	0.169	—	—	0.168	0.168	0.165	0.165
Re 1000							
Mean C_D	1.531	1.408	0.581	1.507	0.205	1.460	0.798
Amplitude C_D	0.236	0.265	0.951	0.199	0.793	0.202	0.732
Mean C_L	0.0	0.0	0.0	0.0	0.0	−0.009	−0.051
Amplitude C_L	1.371	1.426	2.250	1.366	2.366	1.259	1.809
Strouhal no.	0.245	0.196	0.196	0.234	0.234	0.226	0.226

two cylinders show a strong dependence on the Reynolds number compared with the flows past a single cylinder. For the case of flows past two cylinders it is observed that the downstream cylinder, which lies in the wake of the upstream cylinder, experiences very large unsteady forces that can give rise to wake-induced flutter. In some cases, complex vortex introductions result in flows that are temporally periodic in the near wake but not so in the far wake.

ACKNOWLEDGEMENT

Partial support for this work has come from the Department of Science and Technology, India under project DST-AE-95279 with the Department of Aerospace Engineering, IIT Kanpur.

REFERENCES

1. M. M. Zdravkovich, 'Review of flow interference between two circular cylinders in various arrangements', *J. Fluids Engng. Trans ASME*, **99**, 618–633 (1977).
2. S. S. Chen, *Flow-Induced Vibrations of Circular Cylindrical Structures*, Hemisphere, New York, 1987.
3. H. J. Kim and P. A. Durbin, 'Investigation of the flow between a pair of circular cylinders in the flopping regime', *J. Fluid Mech.*, **196**, 431–448 (1988).
4. H. Tokunga, T. Tanaka and N. Satofuka, 'Numerical simulation of viscous flows along multiple bodies by generalized vorticity–stream function formulation', *Comput. Fluid Dyn. J.*, **1**, 58–66 (1992).
5. C. H. K. Williamson, 'Evolution of a single wake behind a pair of bluff bodies', *J. Fluid Mech.*, **159**; 1 (1985).
6. M. Behr T. E. Tezduyar and H. Higuchi, 'Wake interference behind two flat plates normal to the flow: a finite-element study', *Theor. Comput. Fluid Mech.*, **2**, 223–250 (1991).
7. M. Kiya, M. Arie, H., Tamura and H. Mori, 'Vortex shedding from two circular cylinders in staggered arrangement', *J. Fluids Engng. Trans. ASME*, **102**, 166–173 (1980).
8. M. Kiya, O. Mochizuki, Y. Ido, T. Suzuki and T. Arai, 'Flip-flopping around two bluff bodies in tandem arrangement', in H. Eckelmann, J. M. R. Graham, P. Huerre and P. A. Monkewitz (eds), *Bluff-Body Wakes, Dynamics and Instabilities*, Springer, Berlin, 1992, pp. 15–18.
9. A. A. Johnson, T. E. Tezduyar and J. Liou, 'Numerical simulation of flows past periodic arrays of cylinders', *Comput. Mech.*, **11**, 371–383 (1993).
10. T. E. Tezduyar, S. Mittal, S. E. Ray and R. Shih, 'Incompressible flow computations with stabilized bilinear and linear equal-order-interpolation velocity–pressure elements', *Comput. Meth. Appl. Mech. Engng.*, **95**, 221–242 (1992).
11. S. Mittal, 'Stabilized space–time finite element formulations for unsteady incompressible flows involving fluid–body interactions', *Ph.D. Thesis*, University of Minnesota, 1992.
12. M. Behr, J. Liou, R. Shih and T. E. Tezduyar, 'Vorticity-stream function formulation of unsteady incompressible flow past a cylinder: sensitivity of the computed flow field to the location of the outflow boundary', *Int. j. numer. meth. fluids*, **12**, 323–342 (1991).
13. M. Behr, D. Hastreiter, S. Mittal and T. E. Tezduyar, 'Incompressible flow past a circular cylinder: dependence of the computed flow field on the location of the lateral boundaries', *Comput. Meth. Appl. Mech. Engng.*, **123**, 309–316 (1995).
14. T. J. R. Hughes and A. N. Brooks, 'A multi-dimensional upwind scheme with no crosswind diffusion', in T. J. R. Hughes (ed.). *Finite Element Method for Convection Dominated Flows*, AMD Vol. 34, ASME, New York, 1979, pp. 19–35.
15. T. J. R. Hughes and T. E. Tezduyar, 'Finite element methods for first-order hyperbolic systems with particular emphasis on the compressible Euler equations', *Comput. Meth. Appl. Mech. Engng.*, **45**, 217–284 (1984).
16. Y. Saad and M. Schultz, 'GMRES: a generalized minimal residual algorithm for solving nonsymmetric linear systems', *SIAM J. Sci. Stat. Comput.*, **7**, 856–869 (1986).
17. H. Schlichting, *Boundary-Layer Theory*, 7th edn, McGraw-Hill, New York, 1979.
18. M. Behr, A. Johnson, J. Kennedy, S. Mittal and T. E. Tezduyar, 'Computation of incompressible flows with implicit finite element implemenations on the Connection Machine', *Comput. Meth. Appl. Mech. Engng.*, **108**, 99–118 (1993).
19. M. Behr, 'Stabilized finite element methods for incompressible flows with emphasis on moving boundaries and interfaces', *Ph.D. Thesis*, Department of Aerospace Engineering, University of Minnesota, 1992.
20. M. Rosenfeld and D. Kwak, 'Numerical simulation of unsteady incompressible viscous flows in generalized coordinate systems', in D. L. Dwyer, M. Y. Hussaini and R. G. Voigt (eds), *Proc. 11th Int. Conf. on Numerical Methods in Fluid Dynamics*, LNP Vol. 323, Springer, New York, 1989, pp. 506–511.
21. S. Balachandar and R. Mittal, 'Role of three-dimensionality in the near wake of two-dimensional cylinders', in T. S. Mruthyunjaya (ed.), *Mechanics and Thermal Sciences*, AME Vol. II, 1996, pp. 1385–1395.

